

Energy-Efficient Activation and Uplink Transmission for Cellular IoT

Chun-Hung Liu, Yu-Han Shen, and Chia-Han Lee

Abstract—Consider a large-scale cellular network in which base stations (BSs) serve massive Internet-of-Things (IoT) devices. Since IoT devices are powered by a capacity-limited battery, how to prolong their working lifetime is a paramount problem for the success of cellular IoT systems. This paper proposes how to use BSs to manage the active and dormant operating modes of the IoT devices via downlink signaling in an energy-efficient fashion and how the IoT devices perform energy-efficient uplink power control to improve their uplink coverage. We first investigate the fundamental statistical properties of an activation signaling process induced by BSs that would like to activate the devices in their cells, which helps to derive the neat expressions of the true, false and total activation probabilities that reveal joint downlink power control and BS coordination is an effective means to significantly improve the activation performance. We then propose an energy-efficient uplink power control for IoT devices which is shown to save power and ameliorate the uplink coverage probability at the same time. We also propose an energy-efficient downlink power control and BS coordination scheme, which is shown to remarkably improve the activation and uplink coverage performances at the same time.

Index Terms—Internet of things, cellular network, energy-efficient communications, activation, power control, coverage probability, stochastic geometry.

I. INTRODUCTION

Connecting numerous physical things (such as sensors) to the Internet by having them piggyback on cellular networks is a promising way for Internet of Things (IoT) communications since cellular networks are able to provide a seamless coverage of mobile devices, low-cost multicasting and broadcasting services [1]. For example, Long Term Evolution for Machines (LTE-M) is a network standard that enables (IoT) devices to piggyback on existing cellular networks so that the devices with a suitable software update can communicate with the cloud over cellular base stations (BSs). Cellular IoT devices are particularly suitable for *mission-critical* applications in which real-time data transfer makes the difference, e.g., self-driving cars or emergency devices in smart cities [2]–[4]. In addition, densely deploying different kinds of BSs in a heterogeneous cellular network significantly reduces the link budget between devices and their serving BSs so that the devices can use low transmit power for uplink transmission.

Despite these aforementioned advantages of cellular IoT, cellular networks face a serious problem while serving massive

IoT devices operated with capacity-limited batteries. How to make the devices operate in an energy-efficient way so as to prolong their working lifetime is critical. There are essentially two methods to extend the working lifetime of IoT devices. One method is to design low power-consuming and/or energy-harvesting circuits for IoT devices [5] [6]. Although such a circuit design method may largely reduce the power consumption of IoT devices and may allow opportunistically replenish battery power, it incurs high hardware design cost. The other method is to let IoT devices switch between the ON (active) and OFF (dormant) operating modes according to traffic patterns to save power. Such a mode-switched method, in general, is of low complexity and low cost because we only need to design a simple ON-OFF signaling protocol to be implemented by the devices and their serving BSs. Most importantly, this mode-switched method may save much more power than the circuit design method because IoT devices usually have much less uplink traffic and they thus operate in the dormant mode for most of the time, whereas the circuit design method only helps when they are active.

A. Motivation and Prior Work

The mode-switched method can be briefly described as follows. Each BS occasionally broadcasts activation signals to instruct the devices in its cell to switch to the active mode for uplink transmission. Once the activated devices finish the uplink transmission and do not receive activation signals after some time, they automatically switch to the dormant mode. This mode-switched method motivates us to study the following two problems. The first one is how BSs broadcast their activation signals to correctly activate their serving devices. The second one is how the activated devices save their transmit power and improve their uplink transmission performance. Most of the prior works on energy-efficient communications in IoT networks do not address these two problems and mainly focus on power allocation, wireless power transfer and energy-harvesting problems of saving and replenishing the power of IoT devices (typically see [7]–[16]). In reference [8], for example, a distributed wireless power transfer system with or without the frequency and phase synchronization is proposed to charge IoT devices by using power beacons. Reference [9] studied how to do energy-efficient dynamic user scheduling and power allocation by minimizing the total power consumption of a wireless network with massive IoT devices under the constraint on the long-term rate requirements of users. Reference [11] jointly analyzed the downlink and uplink coverage problem of RF-powered IoT devices in a

C.-H. Liu is with the Department of Electrical and Computer Engineering at Mississippi State University, Mississippi State 39762, USA. Y.-H. Shen and C.-H. Lee are with the Institute of Communications Engineering and Department of Electrical and Computer Engineering at National Chiao Tung University, Hsinchu 30010, Taiwan. The corresponding author is Dr. Liu (e-mail: chliu@ece.msstate.edu).

cellular network, but it did not address how to jointly perform downlink and uplink energy-efficient transmission based on the analytical coverage results. In reference [15], a power minimization problem of a simultaneous wireless information and power transfer network with coexisting power-splitting IoT devices and time-switching IoT devices was investigated under a nonlinear energy harvesting model. Although reference [16] studied the RF wake-up problem of IoT devices that is similar to the first problem mentioned above, it does not study how to control the downlink transmit power of BSs to save power and improve the probability of correctly activating the devices as much as possible.

B. Contributions

Since the aforementioned two problems are barely investigated in the literature, this paper is dedicated to thoroughly studying them and its contributions are summarized as follows:

- An activation signaling process in a Poisson cellular network is proposed to characterize the total activation signal power received by a device. The false, true and total activation probabilities are defined based on the activation signaling process, and the Laplace transforms of the activation signaling process and its sub-processes are derived in a form that is easy to compute.
- We adopt the technique of inverse Laplace transform to explicitly find the expressions of the false, true and total activation probabilities for downlink channels with Nakagami- m fading and show that they can be reduced to nearly a closed form when the path-loss exponent is equal to four. From these expressions, we learn that joint downlink power control and BS coordination can effectively increase the true activation probability and reduce the false activation probability at the same time and the activation performance is thus improved.
- An energy-efficient uplink power control scheme is proposed to save power for IoT devices. For the proposed scheme, we not only derive the uplink coverage (probability) for uplink channels with Nakagami- m fading and find its closed form when the path-loss exponent is equal to four, but also show that the scheme is able to save power and improve the uplink coverage at the same time if the system parameters are chosen appropriately.
- We also propose an energy-efficient downlink power control and BS coordination scheme to save power as well as improve the activation performance. The false, true, and total activation probabilities are derived under the proposed scheme, and how the scheme is able to enhance the uplink coverage is shown. Finally, we propose an activation performance index to quantitatively evaluate the activation performance of the proposed scheme under various parameter settings, which can provide insights into how to choose the system parameters for the proposed scheme.

Furthermore, numerical simulation results are provided to validate the correctness and accuracy of our analytical findings and support our observations and discussions.

C. Paper Organization

The rest of this paper is organized as follows. In Section II, the system model and its related assumptions are first specified and then the preliminaries regarding the activation signaling process are introduced. Section III analyzes the total activation probability and uplink coverage with energy-efficient power control. In Section IV, an energy-efficient downlink power control and BS coordination scheme is proposed, and how it affects the activation performance and uplink coverage is studied. Finally, Section V concludes our analytical findings and observations.

II. SYSTEM MODEL AND PRELIMINARIES

Consider a large-scale planar cellular network in which all (small cell) BSs form an independent homogeneous Poisson point process (PPP) of density λ_b and they can be expressed as the set Φ_b given by

$$\Phi_b \triangleq \{X_i \in \mathbb{R}^2 : i \in \mathbb{N}\}, \quad (1)$$

where X_i denotes BS i and its location. Suppose there are numerous (IoT) devices which are randomly and independently distributed over the entire cellular network. These IoT devices form an independent homogeneous PPP of density λ_d and can be represented by the following set:

$$\Phi_d \triangleq \{D_j \in \mathbb{R}^2 : j \in \mathbb{N}\},$$

where D_j denotes device j and its location. All the devices are assumed to simply have two power operating modes similar to the modes proposed in [16]: one is the **active** mode and the other is the **dormant** mode. If the devices are not requested to perform uplink transmission by their serving BSs after some short period of time, they automatically switch to the dormant mode to save power, yet they remain registered in the network. Each BS occasionally sends a signal to activate (wake up) the dormant devices in its cell so as to switch them back to the active mode and requests them to perform uplink transmission. We assume all the IoT devices are served by their nearest BS and all the BSs in the network use the same radio resource (channel) to manage the power operating modes of the IoT devices. According to Lemma 2 in our previous work [17], such a nearest BS association scheme gives rise to the following probability mass function (PMF) of the number of the devices associated with a BS:

$$\phi_n \triangleq \frac{\Gamma(n + \frac{7}{2})}{n! \Gamma(\frac{7}{2})} \left(1 + \frac{2\lambda_d}{7\lambda_b}\right)^{-(n + \frac{7}{2})}, \quad (2)$$

where ϕ_n is the probability that there are n devices associated with a BS and $\Gamma(x) \triangleq \int_0^\infty t^{x-1} e^{-t} dt$ is the Gamma function. The density ratio of λ_d/λ_b in (2) denotes the average number of the devices in a cell since all the cells of the BSs in the network are Voroni-tessellated and each of them has an average area of $1/\lambda_b$ [18] [19]. Note that the density λ_d of the devices is much larger than that of the BSs in practice so that each BS almost surely associates with at least one device and thereby almost no void cells exist in the network [20], [21], i.e., $\phi_0 = (1 + 2\lambda_d/7\lambda_b)^{-\frac{7}{2}} \approx 0$ owing to $\frac{\lambda_d}{\lambda_b} \gg 1$. Thus, the void cell phenomenon due to BS association will not be considered in the following modeling and analysis.

A. Channel Model and activation signaling process

Suppose there is a typical device located at the origin and it is associated with BS $X_1 \in \Phi_b$ that is the nearest BS to it. The channel between a BS and a device undergoes path loss and small-scale fading. Let the transmit power of a BS be constant \bar{P} , and then the total aggregated power of the activation signals from all the BSs received by the typical device can be written as¹

$$W \triangleq \underbrace{\omega_1 \bar{P} H_1 \|X_1\|^{-\alpha}}_{D_1} + \underbrace{\sum_{i: X_i \in \Phi_{b,1}} \omega_i \bar{P} H_i \|X_i\|^{-\alpha}}_{I_1}, \quad (3)$$

where $\omega_i \in \{0, 1\}$ is a Bernoulli random variable (RV) that is unity if BS X_i is transmitting its activation signal and zero otherwise, H_i is the fading channel gain from BS X_i to the typical device, $\|Y_i - Y_j\|$ denotes the Euclidean distance between nodes Y_i and Y_j for $i \neq j$, $\Phi_{b,1} \triangleq \Phi_b \setminus X_1$ is the set of the BSs without X_1 , and $\alpha > 2$ denotes the path-loss exponent. All the small-scale fading channel gains in (3) are assumed to be i.i.d. and they can be characterized by the Nakagami- m fading model² so that $H_i \sim \text{Gamma}(m, m)$ is a Gamma RV with shape m and rate m for all $i \in \mathbb{N}_+$. In this paper, we call W *activation (shot) signaling process* because it captures the cumulative effect at a device of a set of random shock signals appearing at random locations X_i , and $\omega_i \bar{P} H_i \|X_i\|^{-\alpha}$ can be viewed as the impulse function that gives the attenuation of the transmit power of a BS in space [23]. Note that D_1 and I_1 in (3) represent the power of the *desired* activation signal from X_1 and the aggregated power of all the *non-desired* interfering activation signals from all the BSs in set $\Phi_{b,1}$, respectively. When BS X_1 broadcasts an activation signal in its cell, D_1 and I_1 both exist in (3) so that I_1 is able to help X_1 activate its devices in this case. When BS X_1 remains idle, only I_1 exists in (3) and the devices served by X_1 may be accidentally activated if I_1 is sufficiently large. This indicates that I_1 plays a crucial role in activating the devices in a cell and we need to appropriately exploit it so as to boost the activation performance.

B. The Statistical Properties of activation signaling process W

According to the activation signaling process in (3), the total activation probability of a device can be defined as follows:

$$\begin{aligned} \eta_a &\triangleq \mathbb{P}[W \geq \theta_a] = \mathbb{P}[W \geq \theta_a | \omega_1 = 1] \mathbb{P}[\omega_1 = 1] \\ &\quad + \mathbb{P}[W \geq \theta_a | \omega_1 = 0] \mathbb{P}[\omega_1 = 0] \\ &= \mu p_a + (1 - \mu) q_a = q_a + \mu(p_a - q_a), \quad (4) \end{aligned}$$

where θ_a denotes the activation threshold that is the minimum power required to activate a device, $\mu \triangleq \mathbb{P}[\omega_i = 1]$ (and thus

¹ According to the Slivnyak theorem [18], [19], [22], the statistical properties evaluated at the origin are the same as those evaluated at any particular point in a PPP. As such, many of the following equations and derivations are expressed and analyzed based on the origin, the location of the typical device.

² The Nakagami- m fading model is adopted in this paper because it covers several different fading models, such as Rayleigh fading (for $m = 1$), Rician fading with parameter L (for $m = \frac{(L+1)^2}{2L+1}$), no fading (for $m \rightarrow \infty$), and other intermediate fading distributions. In addition, for the tractable analysis in the sequel, m is assumed as a non-negative integer if needed.

$\mathbb{P}[\omega_i = 0] = 1 - \mu$) for all $i \in \mathbb{N}_+$, $p_a \triangleq \mathbb{P}[W \geq \theta_a | \omega_1 = 1]$ is called the *true activation probability*, and $q_a \triangleq \mathbb{P}[W \geq \theta_a | \omega_1 = 0]$ is called the *false activation probability*. Note that p_a reveals how likely a device is successfully activated by the BS associating with it whereas q_a reflects how likely a device is accidentally activated by the BSs not associating with it. Moreover, q_a also indicates whether a device in the network operates in an energy-efficient status in that a small value of q_a implies that devices do not loose much energy due to false activation. As such, an active BS has a high activation performance if it can attain a high true activation probability and a low false activation probability while activating its devices.

To achieve the goal of high activation performance, we need to increase p_a and lower q_a as much as possible. Generally exploiting the statistical properties of the activation signaling process W in (3) sheds light on how to efficiently achieve this goal. In particular, we are interested in the Laplace transforms of W , I_1 and $D_1 + I_1$ because they will facilitate our following analyses and derivations regarding the total activation probability of a device. The Laplace transform of a non-negative RV Z is defined as $\mathcal{L}_Z(s) \triangleq \mathbb{E}[\exp(-sZ)]$ for $s > 0$ and thereby $\mathcal{L}_W(s)$, $\mathcal{L}_{I_1}(s)$ and $\mathcal{L}_{D_1+I_1}(s)$ are explicitly found as shown in the following proposition.

Proposition 1. *For the activation signaling process W in (3), its Laplace transform is found as*

$$\begin{aligned} \mathcal{L}_W(s) &= \exp \left\{ -\frac{\pi \lambda_b \mu (s \bar{P})^{\frac{2}{\alpha}} \Gamma(m + \frac{2}{\alpha}) \Gamma(1 - \frac{2}{\alpha})}{\Gamma(m)} \right\} \\ &= \exp \{ -\pi \lambda_b \mu \mathfrak{J}(0, s \bar{P}) \}, \quad (5) \end{aligned}$$

where $\mathfrak{J}(\cdot, \cdot)$ is defined as

$$\begin{aligned} \mathfrak{J}(x, y) &\triangleq y^{\frac{2}{\alpha}} \frac{\Gamma(m + \frac{2}{\alpha}) \Gamma(1 - \frac{2}{\alpha})}{\Gamma(m)} \\ &\quad - y^{\frac{2}{\alpha}} \int_0^{y^{-\frac{2}{\alpha}} x} \left[1 - \left(\frac{t^{\frac{\alpha}{2}}}{t^{\frac{\alpha}{2}} + m} \right)^m \right] dt. \quad (6) \end{aligned}$$

The Laplace transform of W for given $\omega_1 = 0$, i.e., $\mathbb{E}[\exp(-sW) | \omega_1 = 0] = \mathcal{L}_{I_1}(s)$, can be found as

$$\mathcal{L}_{I_1}(s) = \int_0^\infty \pi \lambda_b \exp \{ -\pi \lambda_b [x + \mu \mathfrak{J}(x, s \bar{P})] \} dx. \quad (7)$$

By using (5) and (7), the Laplace transform of W for given $\omega_1 = 1$, i.e., $\mathbb{E}[\exp(-sW) | \omega_1 = 1] \triangleq \mathcal{L}_{D_1+I_1}(s)$, can be obtained as

$$\mathcal{L}_{D_1+I_1}(s) = \frac{1}{\mu} [\mathcal{L}_W(s) - (1 - \mu) \mathcal{L}_{I_1}(s)]. \quad (8)$$

Proof: See Appendix A. ■

Remark 1. *If the integral in the second term of (6) has $y = s \bar{P}$, then the mean value theorem in Calculus indicates that*

there exists an $x_1 \in [0, (s\bar{P})^{-\frac{2}{\alpha}}x]$ for any $x > 0$ such that the following identity

$$\begin{aligned} & (s\bar{P})^{\frac{2}{\alpha}} \int_0^{(s\bar{P})^{-\frac{2}{\alpha}}x} \left[1 - \left(\frac{t^{\frac{\alpha}{2}}}{t^{\frac{\alpha}{2}} + m} \right)^m \right] dt \\ &= \left(1 - \left[\frac{x_1^{\frac{\alpha}{2}}}{x_1^{\frac{\alpha}{2}} + m} \right]^m \right) x \triangleq \epsilon_1 x \end{aligned}$$

holds for $\epsilon_1 \triangleq 1 - \left[\frac{x_1^{\frac{\alpha}{2}}}{x_1^{\frac{\alpha}{2}} + m} \right]^m$. Thus, there exists an $\epsilon_1 \in [0, 1)$ such that $\mathfrak{J}(x, s)$ in (6) can be equivalently written as

$$\begin{aligned} \mathfrak{J}(x, s\bar{P}) &= (s\bar{P})^{\frac{2}{\alpha}} \frac{\Gamma(m + \frac{2}{\alpha})\Gamma(1 - \frac{2}{\alpha})}{\Gamma(m)} - \epsilon_1 x \\ &= \mathfrak{J}(0, s\bar{P}) - \epsilon_1 x. \end{aligned} \quad (9)$$

In light of this, if ϵ_1 is not sensitive to x (e.g., $m \gg x_1$ and $m \ll x_1$), then (7) approximately reduces to

$$\mathcal{L}_{I_1}(s) \approx \frac{\exp[-\pi\lambda_b\mu\mathfrak{J}(0, s\bar{P})]}{1 - \mu\epsilon_1}. \quad (10)$$

Such an approximation is very accurate, which will be numerically demonstrated in Section III-C.

Note that the closed-form result in (5) is essentially similar to the Laplace transform of the interference of a Poisson wireless ad hoc network in the literature (e.g., see [19], [22]), but it is much more general. Also note that the result in (7) is similar to the result of Theorem 1 in our previous work [24], whereas the result in (8) has not been found in the literature. Although the results in Proposition 2 are not completely found in closed form, they are able to reduce to very neat expressions for some special cases. For example, if $s = x^{\frac{\alpha}{2}}/\bar{P}$ and considering Rayleigh fading (i.e., $m = 1$), then $\mathcal{L}_{I_1}(s)$ in (7) exactly reduces to

$$\mathcal{L}_{I_1}\left(\frac{x^{\frac{\alpha}{2}}}{\bar{P}}\right) = \frac{1}{1 + \mu\mathfrak{J}(1, 1)}, \quad (11)$$

where $\mathfrak{J}(1, 1)$ is given by

$$\mathfrak{J}(1, 1) = \frac{1}{\text{sinc}(2/\alpha)} - \int_0^1 \frac{dt}{1 + t^{\frac{\alpha}{2}}}$$

in which $\text{sinc}(2/\alpha) \triangleq \frac{\sin(2\pi/\alpha)}{2/\alpha} = 1/\Gamma(1 + \frac{2}{\alpha})\Gamma(1 - \frac{2}{\alpha})$ and $\mathcal{L}_{D_1+I_1}(s)$ in (8) can be simply expressed as

$$\mathcal{L}_{D_1+I_1}\left(\frac{x^{\frac{\alpha}{2}}}{\bar{P}}\right) = \frac{1}{\mu} \left\{ \frac{\text{sinc}(2/\alpha)}{\text{sinc}(2/\alpha) + \mu} - \frac{(1 - \mu)}{1 + \mu\mathfrak{J}(1, 1)} \right\}. \quad (12)$$

Note that the results in (11) and (12) do not depend on λ_b . In other words, I_1 and $D_1 + I_1$ scaled by $\|X_1\|^\alpha$ do not depend on λ_b so that densely deploying BSs does not influence the statistical performances of activating devices in this case. This observation motivates us to propose an energy-efficient power control for the devices and the BSs in the following to ameliorate the activation performance of each BS and the uplink coverage performance of each device.

III. ANALYSIS OF TOTAL ACTIVATION PROBABILITY AND UPLINK COVERAGE

As shown in the previous section, the total activation probability consists of the true activation probability and the false activation probability. In this section, we will first analyze the false, true and total activation probabilities and then study how they influence the uplink coverage performance of a device that is correctly activated. Recall that the false activation probability represents how likely the IoT devices are accidentally activated by the interfering active BSs. Thus, the devices that are accidentally activated will interfere the uplink transmissions of the devices that are correctly activated. In other words, the false activation probability considerably affects the uplink transmission performance of the devices. We will finally provide numerical results to validate the derived analytical results pertaining to the total activation probability and the uplink coverage (probability) of a device.

A. Analysis of the Total Activation Probability

In this subsection, we study the false, true and total activation probabilities in a simple context where no any specific techniques for the devices and BSs (such as power control and BS coordination) are employed in the network. The false, true and total activation probabilities in this context are found in the following proposition.

Proposition 2. According to the total activation probability defined in (4), the false activation probability is found as

$$q_a = 1 - \int_0^{\theta_a} \mathcal{L}^{-1} \left\{ \int_0^\infty \pi\lambda_b e^{-\pi\lambda_b[x + \mu\mathfrak{J}(x, s\bar{P})]} dx \right\}(\tau) d\tau, \quad (13)$$

where $\mathcal{L}^{-1}\{F(s)\}(\tau)$ denotes the inverse Laplace transform of function $F(s)$ with parameter $\tau > 0$. The true activation probability is derived as

$$\begin{aligned} p_a &= 1 - \frac{1}{\mu} \int_0^{\theta_a} \mathcal{L}^{-1} \left\{ e^{-\pi\lambda_b\mu\mathfrak{J}(0, s\bar{P})} \right\}(\tau) d\tau \\ &\quad + \frac{(1 - \mu)}{\mu} (1 - q_a). \end{aligned} \quad (14)$$

Thus, the total activation probability defined in (4) is given by

$$\eta_a = 1 - \int_0^{\theta_a} \mathcal{L}^{-1} \left\{ e^{-\pi\lambda_b\mu\mathfrak{J}(0, s\bar{P})} \right\}(\tau) d\tau. \quad (15)$$

Proof: See Appendix B. ■

According to the identity of $\mathfrak{J}(x, y)$ in (9) and the approximate result of $\mathcal{L}_{I_1}(s)$ in (10), the false activation probability in (13) can be approximated by

$$q_a \approx 1 - \frac{1}{1 - \mu\epsilon_1} \int_0^{\theta_a} \mathcal{L}^{-1} \left\{ e^{-\pi\lambda_b\mu\mathfrak{J}(0, s\bar{P})} \right\}(\tau) d\tau, \quad (16)$$

whereas the true activation probability in (14) is approximately given by

$$p_a \approx 1 - \frac{1 - \epsilon_1}{1 - \mu\epsilon_1} \int_0^{\theta_a} \mathcal{L}^{-1} \left\{ e^{-\pi\lambda_b\mu\mathfrak{J}(0, s\bar{P})} \right\}(\tau) d\tau. \quad (17)$$

For the special case of $\alpha = 4$, the integral in (16) and (17) has a closed-form result given by [25]

$$\begin{aligned} & \int_0^{\theta_a} \mathcal{L}^{-1} \left\{ e^{-\pi\mu\lambda_b\mathfrak{J}(0,s\bar{P})} \right\} (\tau) d\tau \\ &= \operatorname{erfc} \left(\frac{\pi^{\frac{3}{2}} \lambda_b \mu \Gamma(m + \frac{1}{2}) \sqrt{\bar{P}}}{2\sqrt{\theta_a} \Gamma(m)} \right), \end{aligned}$$

where $\operatorname{erfc}(z) \triangleq \frac{2}{\sqrt{\pi}} \int_z^\infty e^{-t^2} dt$ is the complementary error function with argument $z \geq 0$. In light of this, when $\alpha = 4$, q_a in (16) and p_a in (17) reduce to the following approximated closed-form results

$$q_a \approx 1 - \frac{1}{(1 - \epsilon_1 \mu)} \operatorname{erfc} \left(\frac{\pi^{\frac{3}{2}} \lambda_b \mu \Gamma(m + \frac{1}{2}) \sqrt{\bar{P}}}{2\sqrt{\theta_a} \Gamma(m)} \right) \quad (18)$$

and

$$p_a \approx 1 - \frac{(1 - \epsilon_1)}{1 - \epsilon_1 \mu} \operatorname{erfc} \left(\frac{\pi^{\frac{3}{2}} \lambda_b \mu \Gamma(m + \frac{1}{2}) \sqrt{\bar{P}}}{2\sqrt{\theta_a} \Gamma(m)} \right), \quad (19)$$

respectively. η_a in (15) reduces to the following exact closed-form expression:

$$\eta_a = \operatorname{erf} \left(\frac{\pi^{\frac{3}{2}} \lambda_b \mu \Gamma(m + \frac{1}{2}) \sqrt{\bar{P}}}{2\sqrt{\theta_a} \Gamma(m)} \right), \quad (20)$$

where $\operatorname{erf}(z) = 1 - \operatorname{erfc}(z)$. To the best of our knowledge, the nearly closed-form results in (18)-(20) that work for different fading models are first derived in this paper. Although the closed-form expressions of q_a , p_a and η_a cannot be found for the case of $\alpha \neq 4$, we can still evaluate them by resorting to numerical techniques.

From the above results of q_a , p_a and η_a , we clearly learn how network parameters λ_b , θ_a , μ , ϵ_1 , and \bar{P} impact the statistics of the activation process. It is fairly easy to see that the three probabilities p_a , q_a and η_a are all dominated by the term $\lambda_b \mu (\bar{P}/\theta_a)^{\frac{3}{2}}$. This indicates that increasing λ_b , μ and \bar{P} increases p_a , q_a and η_a whereas increasing θ_a reduces them. In other words, the methods of densely deploying BSs, frequently activating the devices and using large transmit power all improve these three probabilities. However, none of these methods is guaranteed to ameliorate the activation performance, i.e., simultaneously decreasing the false activation probability and increasing the true activation probability. A possible approach to attaining a high activation performance is to reduce ϵ_1 because (18) and (19) indicate that q_a monotonically decreases and p_a monotonically increases as ϵ_1 increases. Furthermore, from the proof of Proposition 1 and Remark 1, we realize that ϵ_1 is pertaining to the term D_1 in (4) and we can thus increase ϵ_1 by augmenting D_1 . Accordingly, a promising method to augment D_1 in the downlink is to perform *downlink power control* and/or *BS coordination*. Such a method and its related statistics of the activation signal process will be studied in Section III-B. Next, we will analyze the uplink coverage (probability) of the activated devices and see how it is affected by p_a , q_a and η_a . Afterwards, we will provide numerical results in Section III-C to validate the above analytical results of p_a , q_a and η_a .

B. Analysis of the Uplink Coverage

Suppose each of the devices in a cell is allocated a unique resource block (RB) for uplink transmission and each of them begins uplink transmission once activated. Now consider the typical device is activated and then begin to transmit data to BS X_1 . Consider the cellular network is dense and interference-limited so that the signal-to-interference (SIR) at BS X_1 can be written as³

$$\gamma_1 = \frac{Q_1 H_1 \|X_1\|^{-\alpha}}{\sum_{j: D_j \in \Phi_{d,a}} Q_j H_j \|D_j - X_1\|^{-\alpha}}, \quad (21)$$

where Q_j is the transmit power of device D_j and $\Phi_{d,a} \subseteq \Phi_d$ denotes the set of the activated devices using the same RB as the typical device. All Q_j 's are i.i.d. if they are random. Since the activation events of all the devices in the network are independent, all the activated devices form a thinning homogeneous PPP with density $\eta_a \lambda_d$. According to (2), the PMF of the number of the activated devices in a cell can be inferred as

$$\phi_{n,a} = \frac{\Gamma(n + \frac{7}{2})}{n! \Gamma(\frac{7}{2})} \left(1 + \frac{2\eta_a \lambda_d}{7\lambda_b} \right)^{-(n + \frac{7}{2})}, \quad (22)$$

and the probability that there are no devices activated in a cell is $\phi_{0,a} = (1 + 7\eta_a \lambda_d / 2\lambda_b)^{-\frac{7}{2}}$ so that the density of the BSs with at least one activated device is $(1 - \phi_{0,a}) \lambda_b$ and the average number of the activated devices in a cell is $\eta_a \lambda_d / \lambda_b$. Note that each cell almost surely has at least one activated device provided $\eta_a \lambda_d / \lambda_b$ is very large (i.e., $\phi_{0,a} \approx 0$). Suppose the probability that a device is allocated to use any one of the RBs in a cell is the same and equal to $\rho \in (0, 1)$. Hence, the density of $\Phi_{d,a}$ is $\rho \eta_a \lambda_d$ in that all the activated devices in the same cell use different RBs to transmit their data.

According to (21), the uplink coverage (probability) of an activated device is defined as

$$\eta_c \triangleq \mathbb{P}[\gamma_1 \geq \theta_c], \quad (23)$$

where $\theta_c > 0$ is the SIR threshold for successful decoding. It is explicitly derived as shown in the following proposition.

Proposition 3. *If m is a non-negative integer and the fractional moment $\mathbb{E}[Q^a]$ of Q_j exists for $a \in (0, 1)$ and all $j \in \mathbb{N}_+$, then the uplink coverage of the activated devices can be found as*

$$\eta_c = \frac{d^{m-1}}{d\tau^{m-1}} \mathbb{E} \left\{ \frac{\tau^{m-1}}{(m-1)!} \exp \left[-\pi \rho \eta_a \lambda_d \mathfrak{J}(0, 1) \mathbb{E} \left[Q^{\frac{2}{\alpha}} \right] \|X_1\|^2 \left(\frac{m}{\tau Q} \right)^{\frac{2}{\alpha}} \right] \right\} \Big|_{\tau=\theta_c^{-1}}, \quad (24)$$

where $\mathbb{E}\{\cdot\}$ is the operator for taking the average of $\|X_1\|^2$ and $Q^{-\frac{2}{\alpha}}$.

³In practice, a densely-deployed cellular network is interference-limited so that the thermal noise power is very small if compared with the interference in the network. Moreover, using SIR to analyze the SIR-based performance metrics is much more tractable than using signal-to-interference-plus noise ratio (SINR) in a Poisson cellular network, which was pointed out in the literature [26]. In light of the above two reasons, we decide to adopt SIR instead of SINR to analyze the uplink coverage in the following.

Proof: See Appendix C. ■

Remark 2. For Rayleigh fading, η_c in (24) for $m = 1$ reduces to

$$\eta_c = \mathbb{E} \left\{ \exp \left[-\pi \rho \eta_a \lambda_d \mathcal{J}(0, 1) \mathbb{E} \left[Q^{\frac{2}{\alpha}} \right] \|X_1\|^2 \left(\frac{\theta_c}{Q} \right)^{\frac{2}{\alpha}} \right] \right\}, \quad (25)$$

which is lower bounded as

$$\eta_c \geq \exp \left\{ -\pi \rho \eta_a \lambda_d \mathcal{J}(0, 1) \theta_c^{\frac{2}{\alpha}} \mathbb{E} \left[Q^{\frac{2}{\alpha}} \right] \mathbb{E} \left[\|X_1\|^2 Q^{-\frac{2}{\alpha}} \right] \right\} \quad (26)$$

based on Jensen's inequality. Hence, if Q is random and $\mathbb{E} \left[Q^{\frac{2}{\alpha}} \right] \mathbb{E} \left[\|X_1\|^2 Q^{-\frac{2}{\alpha}} \right] \leq \mathbb{E} [\|X_1\|^2] = \frac{1}{\pi \lambda_b}$ holds, the uplink coverage of the activated devices using stochastic transmit power is higher than that of the activated devices using constant transmit power.

Although the uplink coverage in Proposition 3 is somewhat complex, it is very general since it considers stochastic transmit power used by all the activated devices. As pointed out in Remark 2, using stochastic transmit power for each device is able to enhance the uplink coverage. In addition, it is able to save transmit power, which can be explained as follows. First consider the context in which all the activated devices using the same constant transmit power \bar{Q} . In this context of constant uplink power control (i.e., no uplink power control), η_c for Rayleigh fading in (25) reduces to the following closed-form result:

$$\eta_c = \frac{\lambda_b}{\lambda_b + \rho \eta_a \lambda_d \theta_c^{\frac{2}{\alpha}} \mathcal{J}(0, 1)}, \quad (27)$$

which is dominated by $\rho \eta_a \lambda_d \theta_c^{\frac{2}{\alpha}} / \lambda_b$. Now consider another context in which we propose the following uplink (energy-efficient) power control for the typical device

$$Q_1 = \frac{\bar{Q} \|X_1\|^{\alpha \nu}}{\Gamma(1 + \frac{\alpha \nu}{2})} \left[(\pi \lambda_b^{\min})^{\frac{\alpha \nu}{2}} \mathbf{1}(\nu \geq 0) + (\pi \lambda_b^{\max})^{\frac{\alpha \nu}{2}} \times \mathbf{1} \left(-\frac{2}{\alpha} < \nu < 0 \right) \right], \quad (28)$$

where ν is a constant greater than $-\frac{2}{\alpha}$ so as to make $\mathbb{E} \left[Q_1^{\frac{2}{\alpha}} \right]$ and $\Gamma(1 + \frac{\alpha \nu}{2})$ both exist, λ_b^{\max} is the maximum (minimum) density for deploying the BSs, λ_b^{\min} is the minimum density for deploying the BSs, and $\mathbf{1}(\mathcal{A})$ is the indicator function that is unity if event \mathcal{A} is true and zero otherwise. Note that $\lambda_b^{\min} \leq \lambda_b \leq \lambda_b^{\max}$. The mean of Q_1 is given by

$$\mathbb{E}[Q] = \bar{Q} \left[\left(\frac{\lambda_b^{\min}}{\lambda_b} \right)^{\frac{\alpha \nu}{2}} \mathbf{1}(\nu \geq 0) + \left(\frac{\lambda_b}{\lambda_b^{\max}} \right)^{-\frac{\nu \alpha}{2}} \times \mathbf{1} \left(0 > \nu > -\frac{2}{\alpha} \right) \right]. \quad (29)$$

Note that the power control in (28) is energy-efficient if compared with constant (no) power control because it leads

to $\mathbb{E}[Q] \leq \bar{Q}$ if $\nu > -\frac{2}{\alpha}$. Using the proposed uplink power control, η_c in (24) for Rayleigh fading can be found as⁴

$$\eta_c(\nu, n_a) = \int_0^\infty e^{-[n_a \Gamma(1+\nu) u^{(1-\nu)} + u]} du, \quad (30)$$

where $n_a \triangleq \frac{\lambda_d}{\lambda_b} \rho \eta_a \theta_c^{\frac{2}{\alpha}} \mathcal{J}(0, 1)$. Note that $\eta_c(0, n_a) = 1/(1 + n_a)$ is equal to the uplink coverage in (27) for constant (no) power control whereas $\eta_c(1, n_a) = \exp(-n_a)$ is the uplink coverage with channel inversion power control. Since $e^{-n_a} < \frac{1}{1+n_a}$ for $n_a > 0$, the uplink coverage performance of the channel inversion power control is essentially worse than that of the constant power control. Hence, we can conclude the following set of (ν, n_a)

$$\mathcal{V}_a \triangleq \left\{ (\nu, n_a) \in \mathbb{R} \times \mathbb{R}_{++} : \nu > -\frac{2}{\alpha}, \eta_c(0, n_a) \leq \eta_c(\nu, n_a) \right\}, \quad (31)$$

which allows a device using (28) to achieve higher uplink coverage and consume lower average power for the Rayleigh fading case. In other words, when the set \mathcal{V}_a is not empty, the activated devices that control their uplink transmit power by using (28) with $(\nu, n_a) \in \mathcal{V}_a$ can save more power and achieve higher uplink coverage than they merely use constant transmit power. We will numerically validate the above observations regarding the uplink coverage with the uplink energy-efficient power control in the following subsection.

C. Numerical Results and Discussions

In this subsection, simulation results are provided to validate the analyses and observations of the activation probabilities and the uplink coverage in the previous subsections. The network parameters used for simulation are shown in Table I. We first show the simulation results of the activation process in Fig. 1. In Fig. 1(a), we can see all the simulated results of the false activation probability and the true activation probability coincide with their corresponding analytical results in (18) and (19) that are found by using the values of ϵ_1 for different BS densities in Fig. 1(b). Thus, (18) and (19) are very accurate. In addition, (20) is correct since the simulation results of the activation probability perfectly coincide with the analytical results calculated by it. As can be seen in Fig. 1(a), the true activation probability p_a is much higher than the false activation probability q_a for all the BS densities, which is good for the network since a device is more likely to be activated correctly. However, q_a grows much faster than p_a as the BS density increases. For example, $p_a = 0.75$ and $q_a = 0.2$ when $\lambda_b = 8 \times 10^{-5}$ BSs/m² whereas $p_a = 0.89$ and $q_a = 0.36$ when λ_b increases up to 1.2×10^{-4} BSs/m². In this case, q_a increases by 80%, while p_a merely grows by 18.7%, which means the activation performance is getting worse as the network is getting denser. The reason that the activation performance becomes worse as the network gets denser is because the

⁴Note that the uplink coverage in (30) for $\nu = 0$ (i.e., constant (no) power control) is similar to the uplink coverage in some prior works (e.g., see [16]). Thus, we can use the uplink coverage with $\nu = 0$ as a baseline result to compare with the uplink coverage with $\nu \neq 0$.

TABLE I
NETWORK PARAMETERS FOR SIMULATION

Parameter \ Transmitter Type	Base Station (Downlink)	IoT Device (Uplink)
Transmit Power (W) \bar{P}, \bar{Q}	20	0.2
Density (BSs/m ² , devices/m ²) λ_b, λ_d	$1 \times 10^{-5} \sim 1.5 \times 10^{-4}$	$100\lambda_b \sim 500\lambda_b$ (or see figures)
Activation Threshold (μ W) θ_a	0.1	not applicable
SIR Threshold θ_c	not applicable	1
Active Probability of a BS μ	0.25	not applicable
Probability of Using Each RB ρ	not applicable	0.01
Path-loss Exponent α	4	
Minimum BS density (BSs/m ²) λ_b^{\min}	5×10^{-6}	
Maximum BS density (BSs/m ²) λ_b^{\max}	3×10^{-4}	
Nakagami- m Fading	$m = 1$ (Rayleigh Fading)	

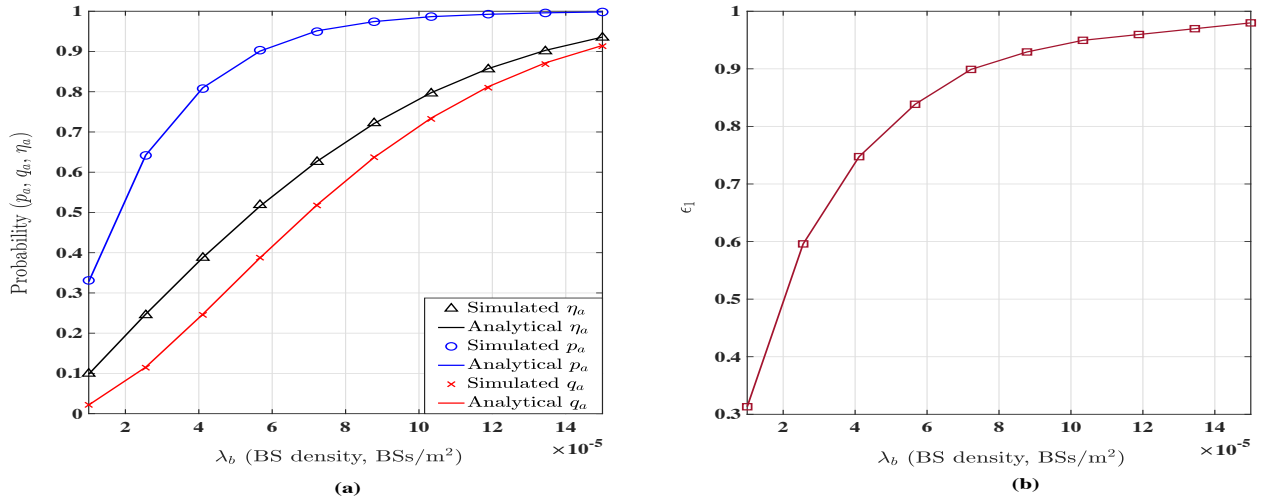


Fig. 1. Simulation results of the activation process: (a) activation probability η , true activation probability p_a and false activation probability q_a versus λ_b , (b) ϵ_1 versus λ_b .

aggregated power of the interfering activation signals increases much faster than the power of the desired activation signal. In the following section, we will propose a downlink power control and BS coordination scheme to improve the activation performance.

Fig. 2 shows the simulation results of the uplink coverage using the uplink power control in (28) for different values of $\frac{\lambda_d}{\lambda_b}$ which represents the average number of the devices associated with a BS. As we can see in the figure, all the analytical results are calculated by using (30) and they perfectly coincide with their corresponding simulated results so that (30) is correct. Also, we can observe that the constant uplink power control with $\nu = 0$ does not always outperform the proposed uplink power control in terms of the uplink coverage. Changing ν significantly impacts the uplink coverage performance of the proposed uplink power control. In the case of $\lambda_b = 1 \times 10^{-5}$ BSs/m² shown in Fig. 2(a), for example, the uplink power control with $\nu = \frac{1}{2}$ is the only one that outperforms the constant power control in the simulation range of $\frac{\lambda_d}{\lambda_b}$. Another case of $\lambda_b = 5 \times 10^{-5}$ BSs/m² shown in Fig. 2(b) further reveals that the proposed uplink power control is not always superior to the constant power control and we should properly choose the value of ν based on λ_b as well as $\frac{\lambda_d}{\lambda_b}$. For instance, the proposed uplink power control

with $\nu = 0.5$ outperforms the constant power control when $100 \leq \frac{\lambda_d}{\lambda_b} \leq 320$, yet it does not perform as well as the constant power control when $\frac{\lambda_d}{\lambda_b} > 320$. Furthermore, we notice that the channel inversion power control (i.e., the case of $\nu = 1$) does not outperform the constant power control so that it is in general not a good option for uplink power control. To visually demonstrate whether there exist some combinations of ν and $\frac{\lambda_d}{\lambda_b}$ that allow the proposed power control to save power and enhance the uplink coverage, the three-dimensional simulation results that show how the uplink coverage varies with ν and $\frac{\lambda_d}{\lambda_b}$ are presented in Fig. 3. As shown in Fig. 3(a), for example, there indeed exists a set of ν and $\frac{\lambda_d}{\lambda_b}$ where the proposed uplink power control outperforms the constant power control so that it can reduce the power consumption and achieve a higher uplink coverage. In other words, we demonstrate that the set in (31) is not empty and indeed exists.

IV. ACTIVATION PROBABILITY AND UPLINK COVERAGE WITH ENERGY-EFFICIENT POWER CONTROL AND BS COORDINATION

The analytical results of the true activation and false activation probabilities found in Section III-A reveal that a possible approach to increasing the true activation probability and reducing the false activation probability at the same time

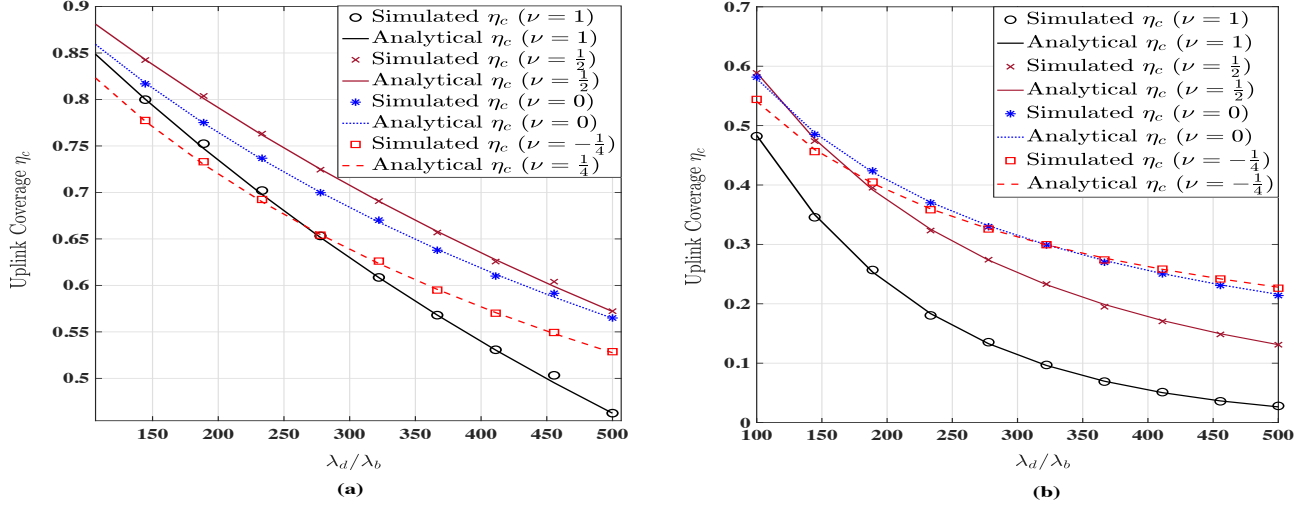


Fig. 2. Simulation results of the uplink coverage probability with the proposed uplink power control for two different values of λ_b : (a) $\lambda_b = 1 \times 10^{-5}$ (BSs/m²), (b) $\lambda_b = 5 \times 10^{-5}$ (BSs/m²).

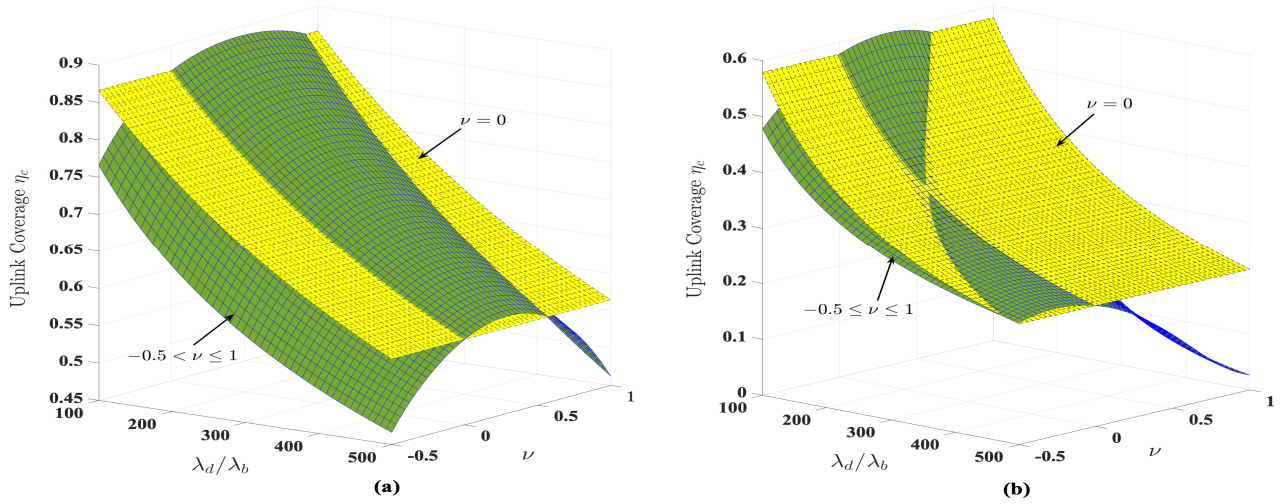


Fig. 3. Simulation results of the uplink coverage probability with the proposed uplink power control for two different values of λ_b : (a) $\lambda_b = 1 \times 10^{-5}$ (BSs/m²), (b) $\lambda_b = 5 \times 10^{-5}$ (BSs/m²).

is to adopt downlink power control and BS coordination. In this section, we will first propose a joint downlink (energy-efficient) power control and BS coordination scheme. We then analyze the true and false activation probabilities and the uplink coverage under such a scheme and show that the proposed scheme is able to improve the activation and uplink coverage performances. Finally, some numerical results will be provided to validate our findings.

A. Activation Process with Downlink Power Control and BS Coordination

According to the uplink power control in (28), it motivates us to propose the following downlink (energy-efficient) power

control for BS X_1 associating with the typical device:

$$P_1 \triangleq \frac{\bar{P} \|X_1\|^{\alpha\beta}}{\Gamma(1 + \frac{\alpha\beta}{2})} \left[(\pi\lambda_b^{\min})^{\frac{\alpha\beta}{2}} \mathbf{1}(\beta \geq 0) + (\pi\lambda_b^{\max})^{\frac{\alpha\beta}{2}} \times \mathbf{1}\left(-\frac{2}{\alpha} < \beta < 0\right) \right], \quad (32)$$

where β is a constant greater than $-\frac{2}{\alpha}$ so as to let $\mathbb{E}[P_1^{\frac{2}{\alpha}}]$ and $\Gamma(1 + \frac{\alpha\beta}{2})$ both exist. Again notice that $P_1 = \bar{P}$ for $\beta = 0$ is the case of constant (no) downlink power control. All the other BSs in the network also independently adopt the same power control scheme as BS X_1 so that all P_i 's are i.i.d. for all $i \in \mathbb{N}_+$. Likewise, the power control in (32) is able to save power for a BS if compared with constant power control since $\mathbb{E}[P_1] = \bar{P} \left[(\frac{\lambda_b^{\min}}{\lambda_b})^{\frac{\alpha\beta}{2}} \mathbf{1}(\beta \geq 0) + (\frac{\lambda_b^{\max}}{\lambda_b})^{\frac{\alpha\beta}{2}} \mathbf{1}(-\frac{2}{\alpha} < \beta < 0) \right] \leq \bar{P}$ so that it is energy-efficient. Moreover, it can reduce

the impact from the BS density on the uplink coverage by properly choosing the value of exponent β owing to $\|X_1\|^2 \sim \exp(\pi\lambda_b)$.

Suppose now the first K nearest BSs to the typical device can be coordinated and synchronized to send their activation signals at the same time by using the downlink power control in (32). Such a joint downlink power control and BS coordination scheme results in another activation signaling process at the typical device similar to W , termed the K th-coordinated activation signaling process, which is defined in the following:

$$W_K \triangleq \omega_1 \underbrace{\left[\sum_{k=1}^K P_k H_k \|X_k\|^{-\alpha} \right]}_{D_K} + \underbrace{\sum_{i: X_i \in \Phi_b^K} \omega_i P_i H_i \|X_i\|^{-\alpha}}_{I_K}, \quad (33)$$

where X_k represents the k th nearest BS in Φ_b to the typical device and $\Phi_{b,K} \triangleq \Phi_b \setminus \{X_k\}_{k=1}^K$. Note that we have $\omega_1 = \dots = \omega_K$ in (33) because the first K nearest BSs to the typical device are coordinated to broadcast their activation signals at the same time. In light of this, D_K represents the sum power of the desired activation signals from the first K nearest BSs whereas I_K stands for the aggregated power of the interfering signals from the BSs in $\Phi_{b,K}$. In other words, W in (3) is essentially equal to W_K in (33) for $K = 1$. The Laplace transform of W_K , which will significantly facilitate our following analyses, can be found as shown in the following proposition.

Proposition 4. *For the K th-coordinated activation signaling process defined in (33), if the fractional moments of P_i and H_i exist, then there exists an $\epsilon_K \in [0, 1)$ such that the Laplace transform of I_K can be approximated by*

$$\mathcal{L}_{I_K}(s) \approx \frac{\exp\left(-\pi\lambda_b\mu\mathcal{J}(0, s)\mathbb{E}\left[P^{\frac{2}{\alpha}}\right]\right)}{(1 - \mu\epsilon_K)^K}, \quad (34)$$

where $\mathbb{E}\left[P^{\frac{2}{\alpha}}\right]$ is given by

$$\mathbb{E}\left[P^{\frac{2}{\alpha}}\right] = \left(\frac{\overline{P}\left[\Gamma(1 + \beta)\right]^{\frac{\alpha}{2}}}{\Gamma(1 + \frac{\alpha\beta}{2})}\right)^{\frac{2}{\alpha}} \left[\left(\frac{\lambda_b^{\min}}{\lambda_b}\right)^{\beta} \mathbf{1}(\beta \geq 0) + \left(\frac{\lambda_b^{\max}}{\lambda_b}\right)^{\beta} \mathbf{1}\left(-\frac{2}{\alpha} < \beta < 0\right) \right], \quad (35)$$

and the Laplace transform of $D_K + I_K$ is approximately derived as

$$\mathcal{L}_{D_K + I_K}(s) \approx [1 - (1 - \mu)\epsilon_K]^K \times \exp\left(-\pi\lambda_b\mu\mathcal{J}(0, s)\mathbb{E}\left[P^{\frac{2}{\alpha}}\right]\right). \quad (36)$$

Using (34) and (36), the Laplace transform of W_K can be found as

$$\mathcal{L}_{W_K}(s) \approx \left[\mu(1 - (1 - \mu)\epsilon_K)^K + \frac{(1 - \mu)}{(1 - \mu\epsilon_K)^K} \exp\left(-\pi\lambda_b\mu\mathcal{J}(0, s)\mathbb{E}\left[P^{\frac{2}{\alpha}}\right]\right) \right]. \quad (37)$$

Proof: See Appendix D. ■

Remark 3. *Note that $\{\epsilon_K\}$ is a monotonic decreasing sequence for all $K \in \mathbb{N}_+$, i.e., $\epsilon_1 > \epsilon_2 > \dots > \epsilon_K > \epsilon_{K+1} > \dots$, based on Remark 1 and we thus have $\lim_{K \rightarrow \infty} \epsilon_K = 0$. Also, note that we can have $\mathbb{E}\left[P^{\frac{2}{\alpha}}\right] \leq \overline{P}^{\frac{2}{\alpha}}$ by choosing an appropriate β such that $\Gamma(1 + \beta) < [\Gamma(1 + \frac{\alpha\beta}{2})]^{\frac{2}{\alpha}}$ holds. This indicates that the downlink power control is also able to reduce the interference I_K .*

According to the definition of I_K in (33), we can infer that $\mathcal{L}_{I_K}(s) > \mathcal{L}_{I_{K-1}}(s) > \dots > \mathcal{L}_{I_1}(s)$ so that we know $(1 - \mu\epsilon_K)^K \leq (1 - \mu\epsilon_1)$ for all $K \in \mathbb{N}_+$ by comparing (34) with (10) and $(1 - \mu\epsilon_K)^K$ decreases as K increases. As a result, $[1 - (1 - \mu)\epsilon_K]^K$ decreases as K increases so that $\mathcal{L}_{D_K + I_K}(s)$ decreases (i.e., $D_K + I_K$ almost surely increases) as K increases. These observations mean that a device gains more activation signal power when its serving BS tries to activate it and it receives less interfering signal power otherwise. Thus, the proposed downlink power control and BS coordination scheme is able to improve the activation performance, which can be explicitly validated in the following proposition in which the true and false activation probabilities are explicitly derived.

Proposition 5. *If the downlink power control in (32) is adopted by all the BSs and the first K nearest BSs to each device are coordinated to activate their devices at the same time, the false activation probability is approximated by*

$$q_a \approx 1 - \frac{1}{(1 - \mu\epsilon_K)^K} \times \int_0^{\theta_a} \mathcal{L}^{-1} \left\{ \exp\left(-\pi\lambda_b\mu\mathcal{J}(0, s)\mathbb{E}\left[P^{\frac{2}{\alpha}}\right]\right) \right\}(\tau) d\tau, \quad (38)$$

the true activation probability is accurately found as

$$p_a \approx 1 - [1 - (1 - \mu)\epsilon_K]^K \times \int_0^{\theta_a} \mathcal{L}^{-1} \left\{ \exp\left(-\pi\lambda_b\mu\mathcal{J}(0, s)\mathbb{E}\left[P^{\frac{2}{\alpha}}\right]\right) \right\}(\tau) d\tau, \quad (39)$$

and the activation probability is accurately given by

$$\eta_a \approx 1 - \left[\mu(1 - (1 - \mu)\epsilon_K)^K + \frac{(1 - \mu)}{(1 - \mu\epsilon_K)^K} \right] \times \int_0^{\theta_a} \mathcal{L}^{-1} \left\{ \exp\left(-\pi\lambda_b\mu\mathcal{J}(0, s)\mathbb{E}\left[P^{\frac{2}{\alpha}}\right]\right) \right\}(\tau) d\tau. \quad (40)$$

Proof: The proof is omitted since it is similar to the proof of Proposition 2. ■

As shown in Proposition 5, if K increases, then $(1 - \mu\epsilon_K)^K$ decreases and q_a in (38) thus reduces. The false probability in (13) without downlink power control and BS coordination is larger than that in (38) for a sufficiently large K . Similarly, if p_a in (39) is compared with the true probability in (14) without downlink power control and BS coordination, then it is certainly larger for a sufficiently large K because $[1 - (1 - \mu)\epsilon_K]^K$ reduces as K increases. Therefore, the proposed downlink power control and BS coordination scheme can improve the activation performance even though it uses smaller average transmit power than the constant power control. In addition,

for $\alpha = 4$, the results in Proposition 5 reduce to the following approximated closed-form results:

$$q_a \approx 1 - \frac{1}{(1 - \mu\epsilon_K)^K} \operatorname{erfc} \left(\frac{\pi^{\frac{3}{2}} \lambda_b \mu \Gamma(m + \frac{1}{2}) \mathbb{E}[\sqrt{P}]}{2\sqrt{\theta_a} \Gamma(m)} \right), \quad (41)$$

$$p_a \approx 1 - [1 - (1 - \mu)\epsilon_K]^K \operatorname{erfc} \left(\frac{\pi^{\frac{3}{2}} \lambda_b \mu \Gamma(m + \frac{1}{2}) \mathbb{E}[\sqrt{P}]}{2\sqrt{\theta_a} \Gamma(m)} \right), \quad (42)$$

and

$$\eta_a \approx 1 - \left[\mu(1 - (1 - \mu)\epsilon_K)^K + \frac{(1 - \mu)}{(1 - \mu\epsilon_K)^K} \right] \times \operatorname{erfc} \left(\frac{\pi^{\frac{3}{2}} \lambda_b \mu \Gamma(m + \frac{1}{2}) \mathbb{E}[\sqrt{P}]}{2\sqrt{\theta_a} \Gamma(m)} \right). \quad (43)$$

Note that (41), (42) and (43) reduce to (18), (19) and (20) for $K = 1$, respectively. Next, we will discuss how the downlink power control and BS coordination scheme impacts the uplink coverage performance and how to properly choose the parameter β in (32) to improve the activation performance.

B. Analysis of the Uplink Coverage and the Activation Performance Index

The uplink coverage derived in (30) clearly shows that it improves as η_a reduces. To make η_a reduce by using the proposed downlink power control and BS coordination scheme, we must have $\frac{d\eta_a}{d\epsilon_K} > 0$ as K increases so that the following inequality has to hold

$$(1 - \mu) \frac{dq_a}{d\epsilon_K} + \mu \frac{dp_a}{d\epsilon_K} > 0$$

since $\eta_a = (1 - \mu)q_a + \mu p_a$. By employing (38) and (39) in the above inequality, we get the following

$$[1 - (1 - \mu)\epsilon_K]^{K-1} (1 - \mu\epsilon_K)^{K+1} < 1, \quad (44)$$

which always holds for all $K \geq 1$ because $[1 - (1 - \mu)\epsilon_K]^{K-1} < 1$ and $(1 - \mu\epsilon_K) < 1$. Therefore, $\frac{d\eta_a}{d\epsilon_K} > 0$ for all $K \geq 1$ and we thus conclude that the proposed downlink power control and BS coordination scheme can benefit the uplink coverage.

We hitherto have shown that the proposed downlink power control and BS coordination scheme not only improve the activation performance but also benefit the uplink coverage. To quantitatively evaluate the activation performance of the proposed downlink power control and BS coordination scheme, we define the activation performance index of an active BS as

$$\zeta_a \triangleq (1 - \eta_a) \left(\frac{p_a}{q_a} - 1 \right), \quad (45)$$

which can be calculated by using (38), (39) and (40). A large value of ζ_a reveals that an active BS has a high activation performance (i.e., it has large p_a as well as small q_a and η_a) because $1 - \eta_a = 1 - q_a[1 + \mu(\frac{p_a}{q_a} - 1)]$ reflects if q_a and η_a are small and the term $(\frac{p_a}{q_a} - 1)$ reveals how much p_a is larger than q_a . We can expound ζ_a in more detail as follows. Consider a

case that each of the active BSs has p_a which is much larger than q_a that is not small. In this case, ζ_a is not large since $1 - \eta_a$ is small and the active BSs thus do not have very good activation performance due to a large q_a even though their p_a is much larger than q_a . Moreover, ζ_a can also indicate whether the active BSs adopt too much downlink power since using large downlink power makes η_a , p_a and q_a approach to unity and may significantly lower ζ_a . We will present numerical results in the following subsection to validate the above analysis and the aforementioned observations.

C. Numerical Results and Discussions

In this subsection, simulation results are provided to validate the previous analyses of the false and true activation probabilities, the uplink coverage and the activation performance index. The network parameters for simulation used in this section are the same as those in Table I. In Fig. 4, we show the simulation results of the K th-coordinated activation signaling process W_K for $K = 2$ when the proposed downlink power control (32) is employed. As can be seen in Fig. 4(a), the analytical results of q_a , p_a and η_a that are calculated by using (41), (42) and (43) with the values of ϵ_2 for different BS densities in Fig. 4(b) are fairly close to their corresponding simulated results. Hence, the approximated results in (41), (42) and (43) are very accurate. Also, we observe that all p_a , q_a and η_a for the case of $\beta = -\frac{1}{4}$ are much larger than those for the case of $\beta = \frac{1}{2}$. This is because the average downlink power for $\beta = -\frac{1}{4}$ is larger than that for $\beta = \frac{1}{2}$. For the case of $K = 3$, the simulation results of q_a , p_a and η_a are shown in Fig. 5 and they can be compared with Fig. 4 to see some interesting differences between them. First, we can observe that p_a increases and q_a decreases as K increases, as expected. Second, η_a and ϵ_K both reduce as K increases so that we validate that $\{\epsilon_K\}$ is a monotonic decreasing sequence (as pointed out in Remark 3) and $\frac{d\eta_a}{d\epsilon_K} > 0$ (as shown in (44)). Third, if we further compare Fig. 1 with Fig. 4 and Fig. 5, we see that the activation performance is significantly improved by the proposed downlink power control and BS coordination scheme as K increases from 1 to 2 whereas it slightly improved as K increases from 2 to 3, which indicates that coordinating two or three BSs in practice would be good enough to significantly enhance the activation performance.

The simulation results of the uplink coverage for uplink power control with different values of ν , downlink power control with $\beta = \frac{1}{2}$ and BS coordination with $K = 3$ are shown in Fig. 6. As we can see in the figure, all simulation results also pretty close to their corresponding analytical results. Also, we can see that all uplink coverage probabilities are significantly improved if they are compared with the simulation results in Fig. 2. This is because the proposed downlink power control and BS coordination scheme reduces the total activation probability η_a so that the interference in the simulation case of Fig. 6 is much smaller than that in the simulation case of Fig. 2. Although Fig. 5 shows that the false, true and total activation probabilities for the downlink power control with $\beta = \frac{1}{2}$ are much smaller than those for the downlink power control with $\beta = -\frac{1}{4}$, the downlink

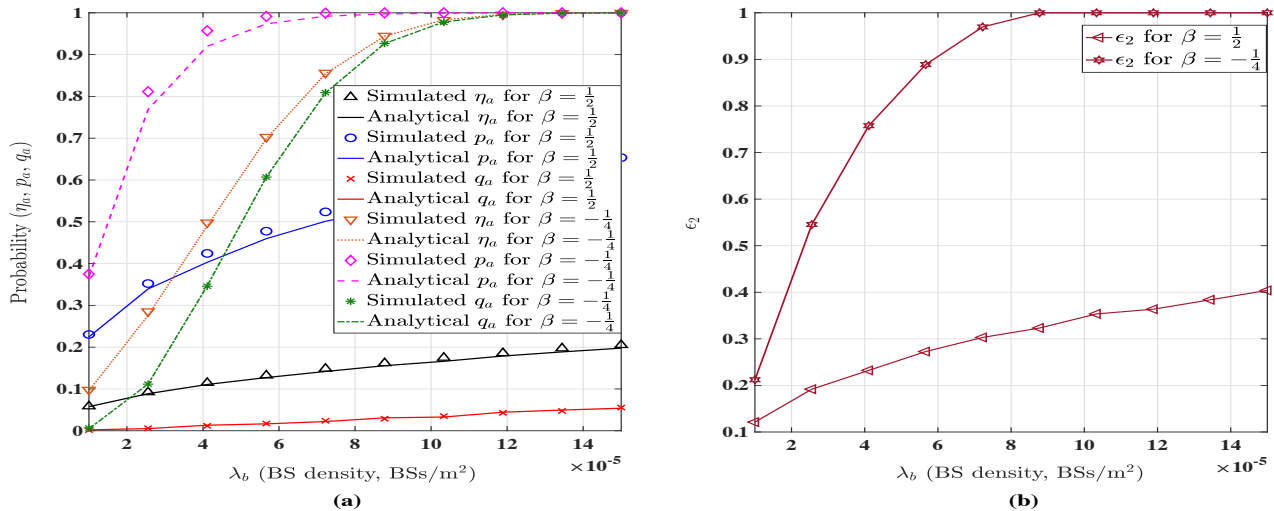


Fig. 4. Simulation results of the second-coordinated activation process with the proposed downlink power control with different values of β : (a) Probabilities η_a , p_a , q_a versus λ_b , (b) ϵ_2 versus λ_b .

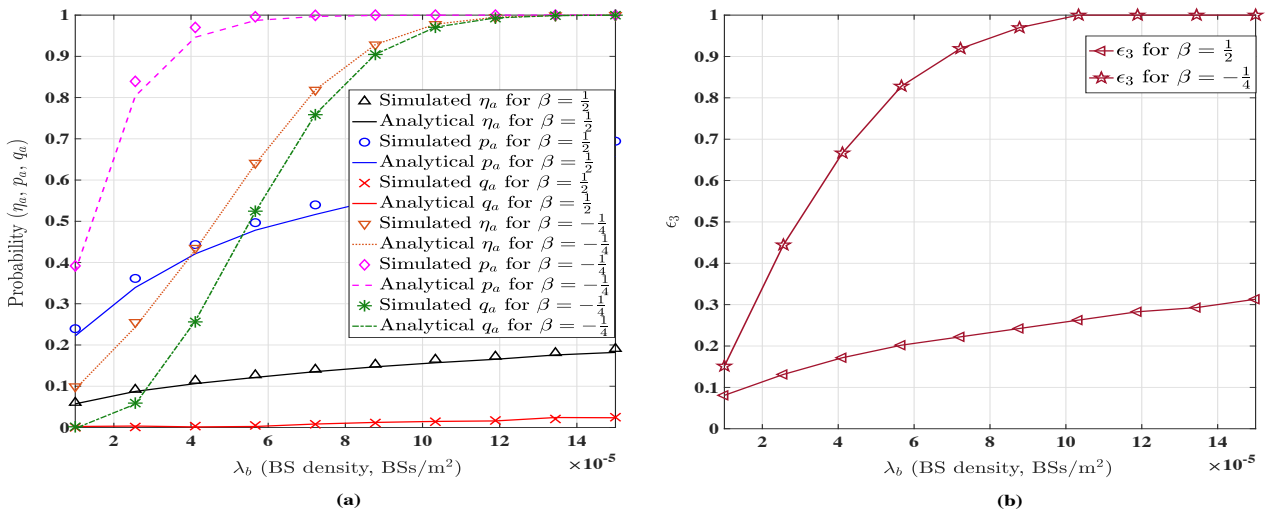


Fig. 5. Simulation results of the third-coordinated activation process with the proposed downlink power control with different values of β : (a) Probabilities η_a , p_a , q_a versus λ_b , (b) ϵ_3 versus λ_b .

power control with $\beta = \frac{1}{2}$ actually outperforms that with $\beta = -\frac{1}{4}$ from the perspective of the activation performance index ζ_a defined in (45). Fig. 7 shows the simulation results of the activation performance index ζ_a for the downlink power control and BS coordination scheme with parameters $\beta \in \{\frac{1}{2}, -\frac{1}{4}\}$ and $K \in \{2, 3\}$. As shown in the figure, the downlink power control with $\beta = \frac{1}{2}$ is much better than that with $\beta = -\frac{1}{4}$ in terms of η_a . As K increases from 2 to 3, η_a remarkably increases. In addition, η_a for the case of $\beta = \frac{1}{2}$ does not vary along λ_b as much as η_a for the case of $\beta = -\frac{1}{4}$. Hence, choosing $\beta = \frac{1}{2}$ is much better than setting $\beta = -\frac{1}{4}$ for the proposed downlink power control in that it attains the much higher performances of activating devices and saving energy. We can use η_a to find the best value of β for the proposed downlink power control.

V. CONCLUSION

Managing the operating modes of IoT devices through BSs is a paramount task since it helps prolong the working lifetime of the devices in a cellular network that are usually powered by capacity-limited batteries. The goal of this paper is to provide insights into how to make the devices operate in an energy-efficient fashion and transmit in an interference-limited environment. To fulfill this goal, we focus on the fundamental analyses of the statistical properties of the activation signaling process generated by the active BSs in the network. We first define the false, true and total activation probabilities and derive their explicit expressions that reveal downlink power control and BS coordination is an effective means to improve the activation performance. We then propose an energy-efficient uplink power control scheme and derive the neat expression of the uplink coverage probability to show

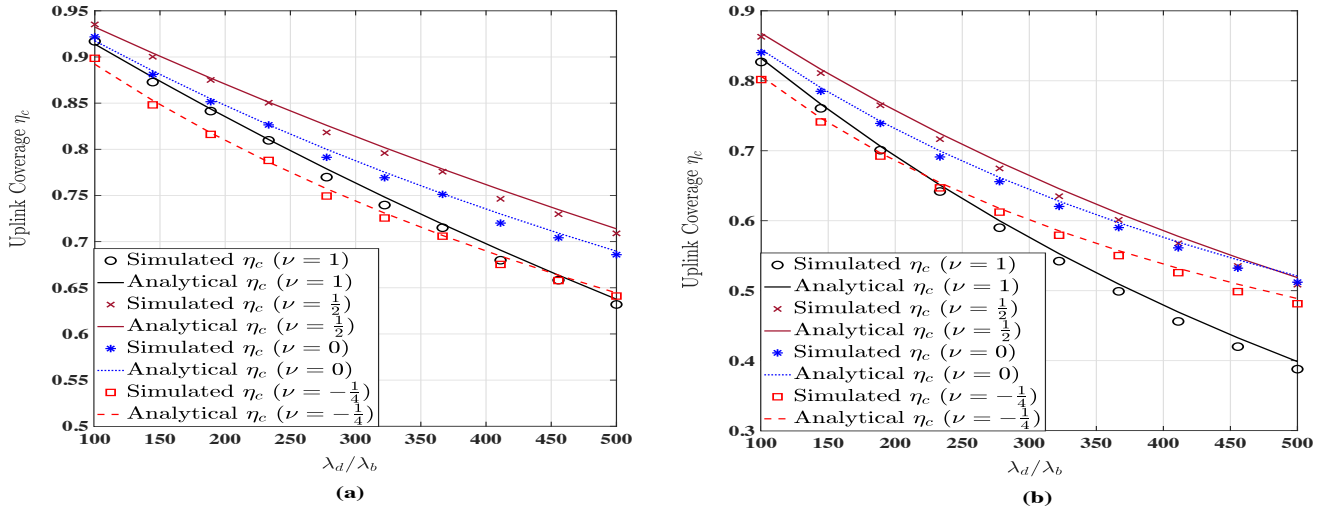


Fig. 6. Simulation results of the uplink coverage probability with the proposed uplink power control and the proposed downlink power control for $\beta = \frac{1}{2}$ and BS coordination scheme with $K = 3$: (a) the case of $\lambda_b = 1 \times 10^{-5}$ (BSs/m²), (b) the case of $\lambda_b = 5 \times 10^{-5}$ (BSs/m²).

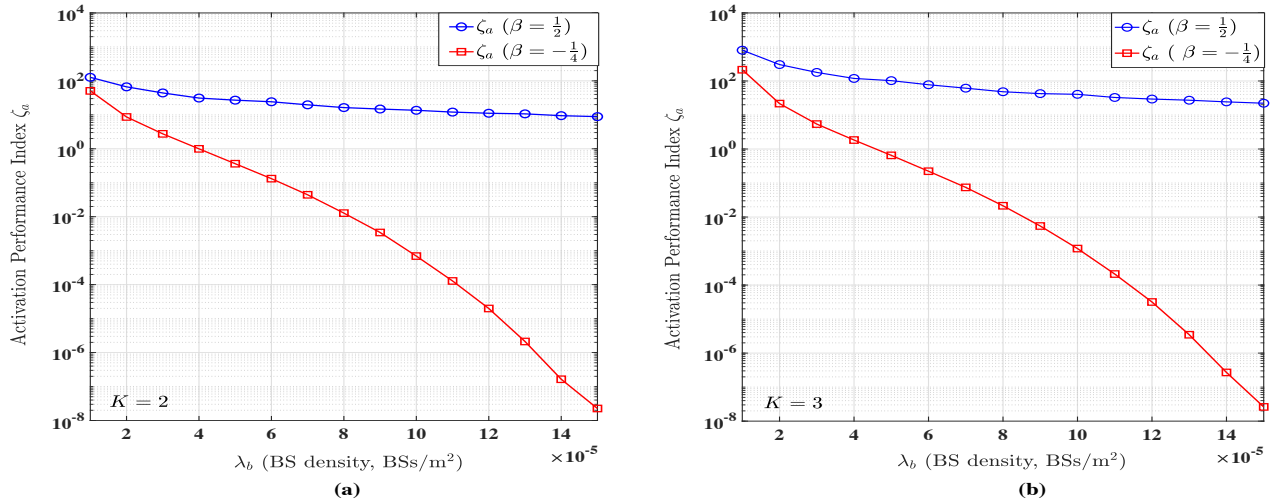


Fig. 7. Simulation results of the activation performance index ζ_a for the proposed downlink power control and BS coordination scheme: (a) ζ_a versus λ_b for the case of $K = 2$, (b) ζ_a versus λ_b for the case of $K = 3$.

its capability of saving power and achieving high uplink coverage. An energy-efficient downlink power control and BS coordination scheme is proposed and it is analytically and numerically validated to be able to save the transmit power of the active BSs, reduce the uplink interference from the activated devices and improve the activation performance.

APPENDIX PROOFS OF PROPOSITIONS

A. Proof of Proposition 1

According to the definition of W in (3) and the conservation property of a PPP in Theorem 1 in [21], we know W can be alternatively expressed as

$$W = \sum_{i: X_i \in \Phi_b} \omega_i \bar{P} H_i \|X_i\|^{-\alpha} \stackrel{d}{=} \sum_{i: \hat{X}_i \in \hat{\Phi}_b} \|\hat{X}_i\|^{-\alpha},$$

where $\stackrel{d}{=}$ stands for the equivalence in distribution, $\hat{\Phi}_b \triangleq \{\hat{X}_i \in \mathbb{R}^2 : \hat{X}_i = (\omega_i \bar{P} H_i)^{-\frac{1}{\alpha}} X_i, X_i \in \Phi_b, i \in \mathbb{N}_+\}$ is a homogeneous PPP of intensity $\lambda_b \mathbb{E}[(\omega \bar{P} H)^{\frac{2}{\alpha}}]$. Thus, the Laplace transform of W can be found as

$$\begin{aligned} \mathcal{L}_W(s) &= \mathbb{E} \left[\exp \left(-s \sum_{i: \hat{X}_i \in \hat{\Phi}_b} \|\hat{X}_i\|^{-\alpha} \right) \right] \\ &= \mathbb{E}_{\hat{\Phi}_b} \left[\prod_{i: \hat{X}_i \in \hat{\Phi}_b} \exp \left(-s \|\hat{X}_i\|^{-\alpha} \right) \right] \\ &\stackrel{(a)}{=} \exp \left[-\pi \lambda_b \mathbb{E} \left[(wPH)^{\frac{2}{\alpha}} \right] \int_0^\infty \left(1 - e^{-sr^{-\frac{\alpha}{2}}} \right) dr \right] \\ &\stackrel{(b)}{=} \exp \left[-\pi \lambda_b \mu(sP)^{\frac{2}{\alpha}} \mathbb{E} \left[H^{\frac{2}{\alpha}} \right] \Gamma \left(1 - \frac{2}{\alpha} \right) \right], \quad (\text{A.1}) \end{aligned}$$

where (a) follows from the probability generating functional (PGFL) of a homogeneous PPP and (b) is due to $\mathbb{E}[(\omega \bar{P}H)^{\frac{2}{\alpha}}] = \mu (sP)^{\frac{2}{\alpha}} \mathbb{E}[H^{\frac{2}{\alpha}}]$. Hence, (5) is obtained because $\mathbb{E}[H^{\frac{2}{\alpha}}] = \Gamma(m + \frac{2}{\alpha})/\Gamma(m)$.

Since X_1 is the nearest BS in Φ_b to the typical device, we know $\|X_{i+1}\|^2 = \|X_1\|^2 + \|X_i\|^2$ for $i > 1$ if X_i the i th nearest BS in Φ_b to the typical device, $\|X_1\|^2 \sim \exp(\pi\lambda_b)$ is an exponential RV with mean $\pi\lambda_b$, and $\|X_i\|^2 \sim \text{Gamma}(i, \pi\lambda_b)$ [27]. Therefore, W in (3) can be equivalently expressed as [21], [24]

$$W \stackrel{d}{=} \frac{\omega_1 \bar{P}H_1}{\|X_1\|^\alpha} + \sum_{j: \tilde{X}_j \in \tilde{\Phi}_b} \frac{\omega_j \bar{P}H_j}{(\|X_1\|^2 + \|\tilde{X}_j\|^2)^{\frac{\alpha}{2}}},$$

where $\tilde{\Phi}_b \triangleq \{\tilde{X}_j \in \mathbb{R}^2 : j \in \mathbb{N}_+\}$ is a homogeneous PPP of intensity λ_b . For given $\omega_1 = 0$ and $\|X_1\|^2 = x$, $\mathcal{L}_{W|\omega_1=0}(s) = \mathcal{L}_{I_1}(s)$ can be expressed as follows:

$$\begin{aligned} \mathcal{L}_{I_1}(s) &= \mathbb{E} \left[\exp \left(- \sum_{j: \tilde{X}_j \in \tilde{\Phi}_b} \frac{s\omega_j \bar{P}H_j}{(x + \|\tilde{X}_j\|^2)^{\frac{\alpha}{2}}} \right) \right] \\ &= \mathbb{E}_{\tilde{\Phi}_b} \left\{ \prod_{j: \tilde{X}_j \in \tilde{\Phi}_b} \mathbb{E} \left[\exp \left(- \frac{s\omega_j \bar{P}H_j}{(x + \|\tilde{X}_j\|^2)^{\frac{\alpha}{2}}} \right) \right] \right\} \\ &\stackrel{(c)}{=} \exp \left\{ -\pi\lambda_b\mu \int_0^\infty \left(1 - \mathbb{E} \left[\exp \left(- \frac{s\bar{P}H}{(x+r)^{\frac{\alpha}{2}}} \right) \right] \right) dr \right\}, \end{aligned} \quad (\text{A.2})$$

where (c) is obtained by applying the probability generating functional (PGFL) of a homogeneous PPP to $\tilde{\Phi}_b$. By letting $R \sim \exp(1)$, the integral in (A.2) can be alternatively expressed as

$$\begin{aligned} &\int_0^\infty \left(1 - \mathbb{E} \left[e^{-\frac{s\bar{P}H}{(x+r)^{\frac{\alpha}{2}}}} \right] \right) dr = \int_0^\infty \mathbb{P} \left[R \leq \frac{s\bar{P}H}{(x+r)^{\frac{\alpha}{2}}} \right] dr \\ &= \int_x^\infty \mathbb{P} \left[u \leq \left(\frac{s\bar{P}H}{R} \right)^{\frac{2}{\alpha}} \right] du = \int_0^\infty \mathbb{P} \left[u \leq \left(\frac{s\bar{P}H}{R} \right)^{\frac{2}{\alpha}} \right] \\ &du - \mathbb{E} \left\{ (s\bar{P})^{\frac{2}{\alpha}} \int_0^{(s\bar{P})^{-\frac{2}{\alpha}}x} \mathbb{P} \left[t \leq \left(\frac{H}{R} \right)^{\frac{2}{\alpha}} \right] dt \right\} \\ &= \mathbb{E} \left\{ (s\bar{P})^{\frac{2}{\alpha}} \mathbb{E} \left[H^{\frac{2}{\alpha}} \right] \mathbb{E} \left[R^{-\frac{2}{\alpha}} \right] \right. \\ &\quad \left. - \int_0^x \left[1 - \left(\frac{t^{\frac{\alpha}{2}}}{t^{\frac{\alpha}{2}} + ms\bar{P}} \right)^m \right] dt \right\}, \end{aligned} \quad (\text{A.3})$$

where (A.3) is equal to (6) since $\mathbb{E}[H^{\frac{2}{\alpha}}]\mathbb{E}[R^{-\frac{2}{\alpha}}] = \frac{\Gamma(m+\frac{2}{\alpha})}{\Gamma(m)}\Gamma(1-\frac{2}{\alpha})$. Substituting (A.3) into (A.2) and averaging over $\|X_1\|^2$ yield the result in (7). Moreover, we know the following

$$\begin{aligned} \mathcal{L}_W(s) &= \mathbb{P}[\omega_1 = 0]\mathcal{L}_{W|\omega_1=0}(s) + \mathbb{P}[\omega_1 = 1]\mathcal{L}_{W_d|\omega_1=1}(s) \\ &= (1-\mu)\mathcal{L}_{I_1}(s) + \mu\mathcal{L}_{D_1+I_1}(s), \end{aligned}$$

which implies the result in (8) since $\mathbb{P}[\omega_1 = 1] = \mu$ and $\mathbb{P}[\omega_1 = 0] = 1 - \mu$. Finally, note $\mathfrak{J}(0, s\bar{P}) = (s\bar{P})^{\frac{2}{\alpha}} \frac{\Gamma(m+\frac{2}{\alpha})}{\Gamma(m)}\Gamma(1-\frac{2}{\alpha})$ based on (6) and we thus get $\mathcal{L}_W(s) = \exp\{-\pi\lambda_b\mu\mathfrak{J}(0, s\bar{P})\}$ in (5), which completes the proof.

B. Proof of Proposition 2

According to (3) and (4), the false activation probability can be explicitly written as

$$\begin{aligned} q_a &= \mathbb{P}[W \geq \theta_a | \omega_0] = 1 - \mathbb{P}[I_1 \leq \theta_a] \\ &= 1 - \mathcal{L}^{-1} \left\{ \frac{1}{s} \mathcal{L}_{I_1}(s) \right\} (\theta_a). \end{aligned}$$

Since $\mathcal{L}^{-1}\{\frac{1}{s}F(s)\}(a) = \int_0^a \mathcal{L}^{-1}\{F(s)\}(\tau)d\tau$ for $a > 0$, the above result of q_a can be expressed as

$$\begin{aligned} q_a &= 1 - \int_0^{\theta_a} \mathcal{L}^{-1}\{\mathcal{L}_{I_1}(s)\}(\tau)d\tau \stackrel{(a)}{=} 1 - \int_0^{\theta_a} \left\{ \int_0^\infty \pi\lambda_b \right. \\ &\quad \left. \times \exp \left\{ -\pi\lambda_b [x + \mu\mathfrak{J}(x, s\bar{P})] \right\} dx \right\} (\tau)d\tau, \end{aligned}$$

where (a) follows from the expression of $\mathcal{L}_{I_1}(s)$ in (7). Thus, the result in (13) is obtained. Next, we know p_a can be written as

$$\begin{aligned} p_a &= \mathbb{P}[W \geq \theta_a | \omega_1] = 1 - \mathbb{P}[D_1 + I_1 \leq \theta_a] \\ &= 1 - \mathcal{L}^{-1} \left\{ \frac{1}{s} \mathcal{L}_{D_1+I_1}(s) \right\} (\theta_a) \end{aligned} \quad (\text{A.4})$$

based on (4). Also, we have

$$\begin{aligned} &\mathcal{L}^{-1} \left\{ \frac{1}{s} \mathcal{L}_{D_1+I_1}(s) \right\} (\theta_a) \\ &= \mathcal{L}^{-1} \left\{ \frac{1}{\mu s} [\mathcal{L}_W(s) - (1-\mu)\mathcal{L}_{I_1}(s)] \right\} (\theta_a) \\ &\stackrel{(b)}{=} \frac{1}{\mu} \mathcal{L}^{-1} \left\{ \frac{1}{s} \exp \left(- \frac{\pi\lambda_b\mu s^{\frac{2}{\alpha}}}{\text{sinc}(2/\alpha)} \mathbb{E} \left[P^{\frac{2}{\alpha}} \right] \right) \right\} (\theta_a) + \frac{(1-\mu)}{\mu} \\ &\quad \times \int_0^\infty \pi\lambda_b e^{-\pi\lambda_b x} \mathcal{L}^{-1} \left\{ \frac{1}{s} e^{-\pi\lambda_b\mu\mathfrak{J}(x, s)} \right\} (\theta_a) dx, \end{aligned} \quad (\text{A.5})$$

where (b) follows from $\mathcal{L}_W(s)$ in (5) and $\mathcal{L}_{I_1}(s)$ in (7). Then substituting (A.5) into (A.4) gives rise to the expression in (14). Finally, the total activation probability can be expressed as

$$\begin{aligned} \eta_a &= 1 - \mathbb{P}[W \leq \theta_a] = 1 - \mathcal{L}^{-1} \left\{ \frac{1}{s} \mathcal{L}_W(s) \right\} (\theta_a) \\ &= 1 - \int_0^{\theta_a} \mathcal{L}^{-1} \{ \mathcal{L}_W(s) \} (\tau)d\tau. \end{aligned} \quad (\text{A.6})$$

Thus, substituting the result in (5) into (A.6) yields the result in (15).

C. Proof of Proposition 3

According to (21) and the Slivnyak theorem, γ_1 can be equivalently evaluated as if X_1 were located at the origin and it can thus be equivalently written as

$$\gamma_1 \stackrel{d}{=} \frac{Q_1 H_1 \|X_1\|^{-\alpha}}{\sum_{j: D_j \in \Phi_{d,a}} Q_j H_j \|D_j\|^{-\alpha}} = \frac{Q_1 H_1}{\|X_1\|^\alpha I_{d,a}},$$

where $I_{d,a} \triangleq \sum_{j:D_j \in \Phi_{d,a}} Q_i H_i \|D_j\|^{-\alpha}$ is the interference from the activated devices in set $\Phi_{d,a}$. By conditioning on $\frac{\|X_1\|^\alpha}{Q_1} = x$, then the uplink coverage can be found as

$$\begin{aligned} \eta_c &= \mathbb{P} \left[\frac{1}{\theta_c} \geq \frac{I_{d,a} \|X_1\|^\alpha}{H_1 Q_1} \mid \frac{\|X_1\|^\alpha}{Q_1} = x \right] \\ &= \mathcal{L}^{-1} \left\{ \frac{1}{s} \mathbb{E} \left[\mathcal{L}_{I_{d,a}} \left(\frac{sx}{H} \right) \right] \right\} \left(\frac{1}{\theta_c} \right). \end{aligned}$$

Furthermore, for any positive real-valued function $\Psi : \mathbb{R}_+ \rightarrow \mathbb{R}_+$ and a non-negative RV Z , we have the following identity:

$$\begin{aligned} \mathbb{E} \left\{ \frac{1}{s} \exp \left[-\Psi \left(\frac{s}{Z} \right) \right] \right\} &= \int_0^\infty \frac{1}{s} \exp \left[-\Psi \left(\frac{s}{z} \right) \right] f_Z(z) dz \\ &= \int_0^\infty \exp \left[-\Psi \left(\frac{1}{t} \right) \right] f_Z(st) dt, \end{aligned} \quad (\text{A.7})$$

where $f_Z(\cdot)$ is the PDF of RV Z . By using the identity in (A.7), we get the following:

$$\begin{aligned} &\frac{1}{s} \mathbb{E} \left[\mathcal{L}_{I_{d,a}} \left(\frac{sx}{H} \right) \right] \\ &= \mathbb{E} \left\{ \frac{1}{s} \exp \left[-\pi \rho \eta_a \lambda_d \mathcal{J}(0, 1) \mathbb{E} \left[Q^{\frac{2}{\alpha}} \right] \left(\frac{sx}{H} \right)^{\frac{2}{\alpha}} \right] \right\} \\ &= \int_0^\infty \exp \left[-\pi \rho \eta_a \lambda_d \mathcal{J}(0, 1) \mathbb{E} \left[Q^{\frac{2}{\alpha}} \right] \left(\frac{x}{t} \right)^{\frac{2}{\alpha}} \right] f_H(st) dt, \end{aligned}$$

where $f_H(st) = \frac{m}{\Gamma(m)} (mst)^{m-1} e^{-mst}$. Therefore, η_c for $\|X_1\|^\alpha / Q_1 = x$ can be obtained by

$$\begin{aligned} \eta_c &= \mathcal{L}^{-1} \left\{ s^{m-1} \int_0^\infty \exp \left[-\pi \rho \eta_a \lambda_d \mathcal{J}(0, 1) \mathbb{E} \left[Q^{\frac{2}{\alpha}} \right] \left(\frac{x}{t} \right)^{\frac{2}{\alpha}} \right] \right. \\ &\quad \left. \frac{m}{\Gamma(m)} (mt)^{m-1} e^{-smt} dt \right\} (x) \\ &= \mathcal{L}^{-1} \left\{ s^{m-1} \mathcal{L} \left\{ \exp \left[-\pi \rho \eta_a \lambda_d \mathcal{J}(0, 1) \mathbb{E} \left[Q^{\frac{2}{\alpha}} \right] \left(\frac{xm}{\tau} \right)^{\frac{2}{\alpha}} \right] \right. \right. \\ &\quad \left. \left. \frac{\tau^{m-1}}{\Gamma(m)} \right\} (s) \right\} (x), \end{aligned}$$

which is exactly the result in (24).

D. Proof of Proposition 4

We define $\tilde{\Phi}_b \triangleq \{\tilde{X}_i \in \mathbb{R}^2 : i \in \mathbb{N}\}$ which is a homogeneous PPP of intensity λ_b and we know $\|X_{i+k}\|^2 = \|X_i\|^2 + \|X_k\|^2$ if X_i is the i th nearest BS in Φ_b to the typical device based on the explanation in the proof of Proposition 1 in Appendix A. Accordingly, $\Phi_{b,K} \triangleq \Phi_b \setminus \{X_k\}_{k=1}^K$ can be equivalently expressed as $\Phi_{b,K} \stackrel{d}{=} \{X_{i+K} \in \Phi_b : \|X_{i+K}\|^2 \stackrel{d}{=} \|\tilde{X}_i\|^2 + \|X_K\|^2, \tilde{X}_i \in \tilde{\Phi}_b, i \in \mathbb{N}_+\}$ so that the Laplace transform of I_K in (33) can be equivalently expressed as

$$\begin{aligned} \mathcal{L}_{I_K}(s) &= \mathbb{E} \left[\exp \left(-s \sum_{i: X_i \in \Phi_{b,K}} \frac{\omega_i P_i H_i}{\|X_i\|^\alpha} \right) \right] \\ &= \mathbb{E} \left[\exp \left(-s \sum_{i: \tilde{X}_i \in \tilde{\Phi}_b} \frac{\omega_i P_i H_i}{(\|X_K\|^2 + \|\tilde{X}_i\|^2)^{\frac{\alpha}{2}}} \right) \right] \end{aligned}$$

$$\begin{aligned} &= \mathbb{E} \left[\prod_{i: \tilde{X}_i \in \tilde{\Phi}_b} \exp \left(-\frac{s \omega_i P_i H_i}{(\|X_K\|^2 + \|\tilde{X}_i\|^2)^{\frac{\alpha}{2}}} \right) \right] \\ &\stackrel{(a)}{=} \mathbb{E}_{\|X_K\|^2} \left[\exp \left\{ -\pi \lambda_b \mu \times \int_{\|X_K\|^2}^\infty \mathbb{E}_{PH} \left[1 - \exp \left(-\frac{sPH}{t^{\frac{\alpha}{2}}} \right) \right] dt \right\} \right], \end{aligned} \quad (\text{A.8})$$

where (a) is obtained by considering that the independence among all ω_i 's is still well preserved after local BS coordination and applying the PGFL of a homogeneous PPP on $\tilde{\Phi}_b$. By letting $R \sim \exp(1)$, the integral in (A.8) for a given $\|X_K\|^2 = x$ can be further simplified as

$$\begin{aligned} \int_x^\infty \mathbb{E}_{PH} \left[1 - \exp \left(-\frac{sPH}{t^{\frac{\alpha}{2}}} \right) \right] dt &= \int_x^\infty \mathbb{P} \left[R \leq \frac{sPH}{t^{\frac{\alpha}{2}}} \right] dt \\ &= \int_x^\infty \mathbb{P} \left[t \leq \left(\frac{sPH}{R} \right)^{\frac{2}{\alpha}} \right] dt \stackrel{(b)}{=} \mathcal{J}(x, sP) \end{aligned}$$

where (b) is obtained based on the results in (A.3) in Appendix A and the definition of $\mathcal{J}(x, sP)$ in (6). According to (9), we can infer that

$$\mathbb{E}[\mathcal{J}(x, sP)] = \mathcal{J}(0, s) \mathbb{E} \left[P^{\frac{2}{\alpha}} \right] - \epsilon_{Kx},$$

where $\mathbb{E}[P^{\frac{2}{\alpha}}]$ is shown in (35) and it is found by using (32) with $\|X_1\|^2 \sim \exp(\pi \lambda_b)$. Therefore, we have

$$\begin{aligned} \mathcal{L}_{I_K}(s) &= \mathbb{E}_{\|X_K\|^2} \left[\exp \left\{ -\pi \lambda_b \mu (\mathcal{J}(0, s) \mathbb{E} \left[P^{\frac{2}{\alpha}} \right] \right. \right. \\ &\quad \left. \left. - \epsilon_K \|X_K\|^2 \right\} \right], \end{aligned} \quad (\text{A.9})$$

which can be approximated by the result in (34) because $\|X_K\|^2 \sim \text{Gamma}(K, \pi \lambda_b)$ and ϵ_K is not sensitive to $\|X_K\|^2$.

According to (33) and the aforementioned results, the Laplace transform of $D_K + I_K$ can be rewritten as follows:

$$\begin{aligned} \mathcal{L}_{D_K + I_K}(s) &= \mathbb{E} \left[\exp \left(-s \sum_{k=1}^K P_k H_k \|X_k\|^{-\alpha} \right. \right. \\ &\quad \left. \left. - s \sum_{i: \tilde{X}_i \in \tilde{\Phi}_b} \frac{\omega_i P_i H_i}{(\|X_K\|^2 + \|\tilde{X}_i\|^2)^{\frac{\alpha}{2}}} \right) \right] = \mathbb{E}_{\|X_K\|^2} \left\{ \exp \left(- \right. \right. \\ &\quad \left. \left. \pi \lambda_b \int_0^{\|X_K\|^2} [1 - \mathcal{L}_{PH}(sr^{-\frac{\alpha}{2}})] dr \right. \right. \\ &\quad \left. \left. - \pi \lambda_b \mu \int_{\|X_K\|^2}^\infty [1 - \mathcal{L}_{PH}(sr^{-\frac{\alpha}{2}})] dr \right) \right\} \\ &= \mathbb{E}_{\|X_K\|^2} \left\{ \exp \left(\pi \lambda_b (1 - \mu) \int_{\|X_K\|^2}^\infty [1 - \mathcal{L}_{PH} \left(\frac{s}{r^{\frac{\alpha}{2}}} \right)] dr \right. \right. \\ &\quad \left. \left. - \pi \lambda_b \int_0^\infty [1 - \mathcal{L}_{PH} \left(\frac{s}{r^{\frac{\alpha}{2}}} \right)] dr \right) \right\} \\ &= \frac{\exp \left[-\pi \lambda_b \mathbb{E} \left[P^{\frac{2}{\alpha}} \right] \mathcal{J}(0, s) \right]}{\mathbb{E} \left\{ \exp \left(-\pi \lambda_b (1 - \mu) \int_{\|X_K\|^2}^\infty [1 - \mathcal{L}_{PH} \left(\frac{s}{r^{\frac{\alpha}{2}}} \right)] dr \right) \right\}} \\ &\stackrel{(c)}{=} \frac{\exp \left[-\pi \lambda_b \mathbb{E} \left[P^{\frac{2}{\alpha}} \right] \mathcal{J}(0, s) \right]}{\mathbb{E} \left[\exp \left\{ -\pi \lambda_b (1 - \mu) (\mathcal{J}(0, s) \mathbb{E} \left[P^{\frac{2}{\alpha}} \right] - \epsilon_K \|X_K\|^2) \right\} \right]}, \end{aligned}$$

where (c) follows from the results in (A.8) and (A.9). The above result of $\mathcal{L}_{D_K+I_K}(s)$ can be approximated by (36) since $\|X_K\|^2 \sim \text{Gamma}(K, \pi\lambda_b)$ and ϵ_K is not sensitive to $\|X_K\|^2$. Furthermore, we know that $\mathcal{L}_{W_{c,K}}(s)$ can be written as

$$\begin{aligned}\mathcal{L}_{W_K} &= \mathbb{P}[\mu_1 = 1] \mathbb{E}[\exp(-sW_K) | \mu_1 = 1] \\ &\quad + \mathbb{P}[\mu_1 = 0] \mathbb{E}[\exp(-sW_{c,K}) | \mu_1 = 0] \\ &= \mu \mathcal{L}_{D_K+I_K}(s) + (1 - \mu) \mathcal{L}_{I_K}(s),\end{aligned}$$

which is approximately equal to the result in (37) owing to (34) and (36).

REFERENCES

- [1] A. Al-Fuqaha, M. Guizani, M. Mohammadi, M. Aledhari, and M. Ayyash, "Internet of things: A survey on enabling technologies, protocols, and applications," *IEEE Commun. Surveys Tuts.*, vol. 17, no. 4, pp. 2347–2376, 4th Quart. 2015.
- [2] A. Zanella, N. Bui, A. Castellani, L. Vangelista, and M. Zorzi, "Internet of things for smart cities," *IEEE Internet Things J.*, vol. 20, no. 1, pp. 22–32, Feb. 2014.
- [3] H. Lu, Q. Liu, D. Tian, Y. Li, H. Kim, and S. Serikawa, "The cognitive internet of vehicles for autonomous driving," *IEEE Netw.*, vol. 33, no. 2, pp. 65–73, Mar./Apr. 2019.
- [4] F. Qi, X. Zhu, G. Mang, M. Kadoch, and W. Li, "UAV network and IoT in the sky for future smart cities," *IEEE Netw.*, vol. 33, no. 2, pp. 96–101, Mar./Apr. 2019.
- [5] X. Liu and N. Ansari, "Toward green IoT: Energy solutions and key challenges," *IEEE Commun. Mag.*, vol. 57, no. 3, pp. 104–110, Mar. 2019.
- [6] A. Frytlog, T. Foss, O. Bakker *et al.*, "Ultra-low power wake-up radio for 5G IoT," *IEEE Commun. Mag.*, vol. 57, no. 3, pp. 111–117, Mar. 2019.
- [7] Z. Chu, F. Zhou, Z. Zhu *et al.*, "Wireless powered sensor networks for internet of things: Maximum throughput and optimal power allocation," *IEEE Internet Things J.*, vol. 5, no. 1, pp. 310–321, Feb. 2018.
- [8] K. W. Choi, A. A. Aziz, D. Setiawan *et al.*, "Distributed wireless power transfer system for internet of things devices," *IEEE Internet Things J.*, vol. 5, no. 4, pp. 2657–2671, Aug. 2018.
- [9] D. Zhai, R. Zhang, L. Cai, B. Li, and Y. Jiang, "Energy-efficient user scheduling and power allocation for NOMA-based wireless networks with massive IoT devices," *IEEE Internet Things J.*, vol. 5, no. 3, pp. 1857–1868, Jun. 2018.
- [10] A. O. Ercan, M. O. Sunay, and I. F. Akyildiz, "RF energy harvesting and transfer for spectrum sharing cellular IoT communications in 5G systems," *IEEE Trans. Mobile Comput.*, vol. 17, no. 7, pp. 1680–1694, Jul. 2018.
- [11] M. A. Kishk and H. S. Dhillon, "Joint uplink and downlink coverage analysis of cellular-based RF-powered IoT network," *IEEE Trans. Green Commun. Netw.*, vol. 2, no. 2, pp. 446–459, Jun. 2018.
- [12] W. Sun and J. Liu, "Coordinated multipoint-based uplink transmission in internet of things powered by energy harvesting," *IEEE Internet Things J.*, vol. 5, no. 4, pp. 2585–2595, Aug. 2018.
- [13] D. S. Gurjar, H. H. Nguyen, and H. D. Tuan, "Wireless information and power transfer for IoT applications in overlay cognitive radio networks," *IEEE Internet Things J.*, vol. 6, no. 2, pp. 3257–3270, Apr. 2019.
- [14] D. Sikeridis, E. E. Tsiropoulou, M. Devetsikiotis, and S. Papavassiliou, "Energy-efficient orchestration in wireless powered internet of things infrastructures," *IEEE Trans. Green Commun. Netw.*, vol. 3, no. 2, pp. 317–328, Jun. 2019.
- [15] R. Jiang, K. Xiong, P. Fan, Y. Zhang, and Z. Zhong, "Power minimization in SWIPT networks with coexisting power-splitting and time-switching users under nonlinear EH model," *IEEE Internet Things J.*, pp. 1–16, Early Access 2019.
- [16] N. Kouzayha, Z. Dawy, J. G. Andrews, and H. ElSawy, "Joint downlink/uplink RF wake-up solution for IoT over cellular networks," *IEEE Trans. Wireless Commun.*, vol. 17, no. 3, pp. 1574–1588, Mar. 2018.
- [17] C.-H. Liu and H.-C. Tsai, "Traffic management for heterogeneous networks with opportunistic unlicensed spectrum sharing," *IEEE Trans. Wireless Commun.*, vol. 16, no. 9, pp. 5717–5731, Sep. 2017.
- [18] S. N. Chiu, D. Stoyan, W. S. Kendall, and J. Mecke, *Stochastic Geometry and Its Applications*, 3rd ed. New York: John Wiley and Sons, Inc., 2013.
- [19] F. Baccelli and B. Błaszczyszyn, "Stochastic geometry and wireless networks: Volume I: Theory," *Foundations and Trends in Networking*, vol. 3, no. 3-4, pp. 249–449, 2010.
- [20] C.-H. Liu and L.-C. Wang, "Random cell association and void probability in Poisson-distributed cellular networks," in *Proc. IEEE Int. Conf. on Commun.*, Jun. 2015, pp. 2816–2821.
- [21] —, "Optimal cell load and throughput in green small cell networks with generalized cell association," *IEEE J. Sel. Areas Commun.*, vol. 34, no. 5, pp. 1058–1072, May 2016.
- [22] M. Haenggi and R. K. Ganti, "Interference in large wireless networks," *Foundations and Trends in Networking*, vol. 3, no. 2, pp. 127–248, 2009.
- [23] S. B. Lowen and M. C. Teich, "Power-law shot noise," *IEEE Trans. Inf. Theory*, vol. 36, no. 6, pp. 1302–1318, Sep. 1990.
- [24] C.-H. Liu and C.-S. Hsu, "Fundamentals of simultaneous wireless information and power transmission in heterogeneous networks: A cell load perspective," *IEEE J. Sel. Areas Commun.*, vol. 37, no. 1, pp. 100–115, Jan. 2019.
- [25] M. Abramowitz and I. A. Stegun, *Handbook of mathematical functions: with formulas, graphs, and mathematical tables*. Courier Dover Publications, 2012.
- [26] C.-H. Liu, "Coverage-rate tradeoff analysis in mmwave heterogeneous cellular networks," *IEEE Trans. Commun.*, vol. 67, no. 2, pp. 1720–1736, Feb. 2019.
- [27] M. Haenggi, *Stochastic Geometry for Wireless Networks*, 1st ed. Cambridge University Press, 2012.